

Hadronic Vacuum Polarization and the MUonE proposal

David Greynat¹ Eduardo de Rafael²

¹*No affiliation at present*

²*Aix-Marseille Univ, Université de Toulon, CNRS, CPT, Marseille, France*

E-mail: david.greynat@gmail.com, EdeR@cpt.univ-mrs.fr

ABSTRACT: The MUonE proposal at the CERN SPS consists in extracting the value of the hadronic vacuum polarization self-energy function (HVP) from its contribution to the differential cross-section of elastic muon-electron scattering. The HVP contribution to the muon anomalous magnetic moment can then be obtained from a weighted integral of the measured HVP self-energy function. This, however, requires a knowledge of the HVP function in its full integration domain. This paper discusses a procedure to reconstruct the HVP function in the regions not directly accessible to measurement. The method is based on the so-called transfer theorems, due to Flajolet and Odlyzko, which we explain and adapt to HVP.

Contents

1	Introduction	1
2	Some Properties of HVP	4
2.1	Conformal Mapping	5
2.2	The Imaginary Part	7
3	Reconstruction Approximants of the HVP Function	9
3.1	Approximants from Asymptotic Freedom	11
3.2	Asymptotic freedom and Lowest Order χ PT	12
4	Reconstruction Approximants for the MUonE Proposal	14
5	Illustration with a Phenomenological Model	16
5.1	Approximants with L=1 only	18
5.2	Reconstruction Approximants with Threshold Constraints	19
6	Conclusions and Outlook	20
A	QED Vacuum Polarization as a Theoretical Laboratory	21
A.1	Reconstruction Approximants in the QED Example	22
A.2	Reconstruction Approximants of the QED Spectral Function	24
B	Results on Combinatorial Analysis	25
B.1	Transfer Theorem	25
B.2	Relation between the \mathcal{B} -coefficients and the \mathcal{R} -residues	28

1 Introduction

The measurements of the anomalous magnetic moment of the muon a_μ , made at BNL [1] and more recently at Fermilab [2, 3], give the results:

$$a_\mu^{\text{BNL}} = 116\,592\,089(63) \times 10^{-11} \quad \text{and} \quad a_\mu^{\text{FNAL}} = 116\,592\,040(54) \times 10^{-11}. \quad (1.1)$$

They agree with each other at the level of 0.6 standard deviations (0.6σ) and their combined number

$$a_\mu(2021) = 116\,592\,061(41) \times 10^{-11}, \quad (1.2)$$

has the remarkable accuracy of 0.35 parts per million.

The theoretical evaluation of the same observable in the Standard Model has been made to a comparable precision. The result

$$a_\mu(\text{Th.WP}) = 116\,591\,810(43) \times 10^{-11} \quad (1.3)$$

is the *consensus theory number* reported in the 2020 White Paper (WP) of ref. [4]. When compared to the experimental number in Eq. (1.2) it turns out to be 4.2σ below, a significant difference, which has triggered many speculations in the literature [5] on what kind of new physics could explain this difference.

The situation at present, however, is rather confusing. The same day that the results of the Fermilab muon g-2 collaboration were published, the journal Nature also published a new result of the Budapest-Marseille-Wuppertal (BMW) lattice QCD (LQCD) collaboration on the lowest order hadronic vacuum polarization contribution to the muon g-2. Their result [6]

$$a_\mu(\text{HVP})_{\text{BMW}} = 7\,075(55) \times 10^{-11}, \quad (1.4)$$

differs from previous evaluations using data-driven dispersion relations [7, 8]:

$$a_\mu(\text{HVP})_{\text{lowest order}}^{\text{ref.}[7]} = 6\,940(40) \times 10^{-11} \quad \text{and} \quad a_\mu(\text{HVP})_{\text{lowest order}}^{\text{ref.}[8]} = 6\,928(24) \times 10^{-11}, \quad (1.5)$$

which are incorporated in the *consensus theory number* given above. The BMW-lattice QCD result reduces the total discrepancy with the experimental result in Eq. (1.2) from 4.2σ to 1.6σ . Still a discrepancy, but not significant to argue evidence for new physics. The result is under detailed examination and one hopes to have news on that in the near future. If the disagreement between LQCD and the experimental dispersive evaluations of the HVP persists, one will have to find the explanation for that. Because they involve integrals of different quantities, comparison of the two methods is difficult, although not impossible.

In the meantime, the Fermilab Muon g-2 experiment expects to reduce the error by a factor of four over the next four years, as more statistics accumulate. There is also a new experiment at the Japan Proton Accelerator Research Complex in Tokai, the J-PARC experiment E34 [9], which will employ a new different technique to measure the muon anomaly.

Another expected experiment is the MUonE proposal at the CERN SPS [10–12]. It consists in extracting the value of the HVP self-energy function in the Euclidean, from its contribution to the differential cross-section of elastic muon-electron scattering with muons at $E_\mu = 160$ GeV colliding on atomic electrons of a fixed low Z target [13]. The muon anomaly can then be obtained from a weighted integral of the measured HVP self-energy function discussed below. The purpose of this paper is to present theoretical arguments concerning this interesting proposal which should increase its potential impact.

The function we shall be concerned with is the Fourier transform of the vacuum expectation value of the time-ordered product of two electromagnetic hadronic currents of the Standard Model $J_\mu^{\text{had}}(x)$ at two separate space-time x -points ($g_{\mu\nu} = \text{diag}(1, -1, -1, -1)$):

$$\Pi_{\mu\nu}^{\text{had}}(q) = i \int_{-\infty}^{+\infty} d^4x \, e^{iq \cdot x} \langle 0 | T \left(J_\mu^{\text{had}}(x) J_\nu^{\text{had}}(0) \right) | 0 \rangle = (q_\mu q_\nu - q^2 g_{\mu\nu}) \Pi_{\text{had}}(q^2). \quad (1.6)$$

The photon hadronic self-energy function $\Pi_{\text{had}}(q^2)$ is a complex function of its q^2 variable. It is an analytic function in the full complex plane, but for a cut in the real axis which

goes from the physical threshold at $q^2 = 4m_{\pi^\pm}^2 \equiv t_0$ to infinity¹ As such, the on-shell renormalized HVP-function, i.e. $\Pi_{\text{had}}(q^2)$ subtracted at its value at $q^2 = 0$, obeys the dispersion relation:

$$\Pi^{\text{HVP}}(q^2) \equiv \Pi_{\text{had}}(q^2) - \Pi_{\text{had}}(0) = \int_{t_0}^{\infty} \frac{dt}{t} \frac{q^2}{t - q^2 - i\epsilon} \frac{1}{\pi} \text{Im}\Pi_{\text{had}}(t), \quad t_0 \equiv 4m_{\pi^\pm}^2. \quad (1.7)$$

The optical theorem relates the hadronic spectral function $\frac{1}{\pi} \text{Im}\Pi_{\text{had}}(t)$ to the observable one-photon annihilation cross-section:

$$\sigma(t)_{e^+e^- \rightarrow \text{had}} \underset{m_e \rightarrow 0}{\sim} \frac{4\pi^2\alpha}{t} \frac{1}{\pi} \text{Im}\Pi_{\text{had}}(t), \quad (1.8)$$

and this is the way that experimental data-driven determinations of $\frac{1}{\pi} \text{Im}\Pi_{\text{had}}(t)$ have been obtained, as well as the evaluation of the anomalous magnetic moment of the muon a_μ^{HVP} , via the integral representation [14–16]

$$a_\mu^{\text{HVP}} = \frac{\alpha}{\pi} \int_{t_0}^{\infty} \frac{dt}{t} \int_0^1 dx \frac{x^2(1-x)}{x^2 + \frac{t}{m_\mu^2}(1-x)} \frac{1}{\pi} \text{Im}\Pi_{\text{had}}(t). \quad (1.9)$$

An alternative representation of a_μ^{HVP} in terms of the hadronic self-energy function $\Pi_{\text{had}}(q^2)$ in the Euclidean ($Q^2 \equiv -q^2 \geq 0$), proposed in refs. [17, 18], follows from a rearrangement of the integrand in Eq. (1.9) and the use of the dispersion relation in Eq. (1.7):

$$\begin{aligned} a_\mu^{\text{HVP}} &= \frac{\alpha}{\pi} \int_0^1 dx (1-x) \int_{t_0}^{\infty} \frac{dt}{t} \frac{\frac{x^2}{1-x} m_\mu^2}{t + \frac{x^2}{1-x} m_\mu^2} \frac{1}{\pi} \text{Im}\Pi_{\text{had}}(t), \\ &= -\frac{\alpha}{\pi} \int_0^1 dx (1-x) \Pi^{\text{HVP}} \left(-\frac{x^2}{1-x} m_\mu^2 \right), \quad Q^2 \equiv \frac{x^2}{1-x} m_\mu^2. \end{aligned} \quad (1.10)$$

This x -Feynman parametric representation is particularly relevant to the MUonE proposal². It requires, however, the knowledge of the x -integrand in Eq. (1.10) in its full range and the experiment can only provide precise enough data in a limited x -window ($x_{\text{min}} \simeq 0.3$ to $x_{\text{max}} \simeq 0.9$). The obvious question which then arises is what reliable method can be used to extrapolate the determination in the x -window to the full x -integration domain. The purpose of this paper is to present a systematic approximation procedure to achieve this reconstruction. It is based on what in the mathematical literature is known as the transfer theorems of Flajolet and Odlyzko [20]³. We shall refer to this as the procedure of *reconstruction approximants*.

In the next section we review some of the HVP properties that we shall be using. The

¹In the presence of higher order electromagnetic corrections the threshold is at the mass of the π^0 because of the $\pi^0\gamma$ contribution to the spectral function. In this paper the threshold is fixed at $t_0 = 4m_{\pi^\pm}^2$, but can be adjusted to $m_{\pi^0}^2$ if necessary.

²It has also been proposed for lattice QCD evaluations in ref. [19].

³For a comprehensive exposition and related subjects see ref. [21], in particular Part B. Complex Asymptotics.

transfer theorem adapted to HVP is discussed in section 3⁴. In section 4 we explain how to apply *reconstruction approximants* in the case of the MUonE proposal, and in section 5 we illustrate this with a phenomenological model. Conclusions and outlook are given in Section 6.

Appendix A is dedicated to showing how the *reconstruction approximants* work in the case of the QED vacuum polarization at the one loop level, where all the steps can be followed analytically. Appendix B contains technical details on combinatorial analysis, which have been used to derive some of the results in the text.

Readers who are only interested in the applications of *reconstruction approximants* are advised to concentrate their attention on sections 4 and 5.

2 Some Properties of HVP

We shall often refer to the Mellin Transform of the hadronic spectral function

$$\mathcal{M}^{\text{HVP}}(s) = \int_{t_0}^{\infty} \frac{dt}{t} \left(\frac{t}{t_0} \right)^{s-1} \frac{1}{\pi} \text{Im} \Pi_{\text{had}}(t), \quad -\infty \leq \text{Re}(s) < 1, \quad (2.1)$$

with its domain of definition extended to the full complex s -plane by analytic continuation. The Mellin Transform $\mathcal{M}^{\text{HVP}}(s)$ is then a meromorphic function with poles in the real axis at $\text{Re}(s) \geq 1$.

Inserting the identity:

$$\frac{1}{1+A} = \frac{1}{2\pi i} \int_{c_s - i\infty}^{c_s + i\infty} ds A^{-s} \Gamma(s) \Gamma(1-s) \quad \text{with} \quad A \equiv \frac{Q^2}{t_0} \quad \text{and} \quad c_s \equiv \text{Re}(s) \in]0, 1[, \quad (2.2)$$

in the integrand of the dispersion relation in Eq. (1.7), the HVP self-energy in the Euclidean ($Q^2 \geq 0$) can then be expressed in terms of the Mellin-Barnes integral⁵

$$\Pi^{\text{HVP}}(-Q^2) = -\frac{Q^2}{t_0} \frac{1}{2\pi i} \int_{c_s - i\infty}^{c_s + i\infty} ds \left(\frac{Q^2}{t_0} \right)^{-s} \Gamma(s) \Gamma(1-s) \mathcal{M}^{\text{HVP}}(s), \quad c_s \equiv \text{Re}(s) \in]0, 1[. \quad (2.3)$$

The region $\text{Re}(s) \in]0, 1[$ in the complex s -plane is called the *fundamental strip*, where the integral converges absolutely. Two basic properties of this representation follow:

- The Taylor expansion of $\Pi^{\text{HVP}}(-Q^2)$ at small Q^2 is governed by the *singular series expansion* of the integrand in Eq. (2.3) at the *left* of the *fundamental strip*, i.e. $\text{Re}(s) \leq$

⁴Another application of transfer theorems, within the context of heavy quarks in QCD, can be found in refs. [22–24].

⁵Mellin-Barnes representations have been extensively discussed in ref. [25] and, within the context of HVP and $g_\mu - 2$, in ref. [26] and references therein. The precise definitions of *fundamental strip* and *singular series* can be found in ref. [25].

0. In this case, the *singular series* is generated by the poles at $s = 0, -1, -2, -3, \dots$ of the $\Gamma(s)$ function in the integrand, with the result:

$$\Pi^{\text{HVP}}(-Q^2) \underset{Q^2 < t_0}{\sim} - \left(\frac{Q^2}{t_0} \right) \left[\sum_{n=0}^{\infty} \left(\frac{Q^2}{t_0} \right)^n (-1)^n \mathcal{M}^{\text{HVP}}(-n) \right], \quad (2.4)$$

where $\mathcal{M}^{\text{HVP}}(-n)$ are the moments of the spectral function:

$$\mathcal{M}^{\text{HVP}}(1-n) = \int_{t_0}^{\infty} \frac{dt}{t} \left(\frac{t_0}{t} \right)^n \frac{1}{\pi} \text{Im} \Pi_{\text{had}}(t), \quad n = 1, 2, 3, \dots, \quad (2.5)$$

clearly accessible to experimental determination up to high- t values, beyond which, perturbative QCD (pQCD) can be used.

- By contrast, the asymptotic expansion of $\Pi^{\text{HVP}}(-Q^2)$ at large- Q^2 is governed by the *singular series expansion* of the integrand in Eq. (2.3) at the *right* of the *fundamental strip*, i.e. $\text{Re}(s) \geq 1$. This is a series of the form:

$$\Gamma(s)\Gamma(1-s) \mathcal{M}^{\text{HVP}}(s) \asymp \sum_{\mathbf{p}=1,2,3,\dots} \sum_{k=0,1,2,\dots} \frac{\mathcal{R}_{\mathbf{p},k}}{(s-\mathbf{p})^{k+1}}, \quad (2.6)$$

with $\mathcal{R}_{\mathbf{p},k}$ the residues of the singularities at $s = \mathbf{p}$ with $k+1$ -multiplicity. The resulting expansion is then:

$$\Pi^{\text{HVP}}(-Q^2) \underset{\frac{Q^2}{t_0} \rightarrow \infty}{\sim} - \frac{Q^2}{t_0} \sum_{\mathbf{p}=1,2,3,\dots} \sum_{k=0,1,2,\dots} \frac{(-1)^{k+1}}{k!} \mathcal{R}_{\mathbf{p},k} \left(\frac{Q^2}{t_0} \right)^{-\mathbf{p}} \log^k \frac{Q^2}{t_0}, \quad (2.7)$$

with the residues $\mathcal{R}_{\mathbf{p},k}$ becoming the coefficients of the large- Q^2 asymptotic expansion. These residues encode complementary information about the hadronic spectral function to the one provided by the moments in Eq. (2.5), though they are not so easily accessible to experimental determination. The terms with one $\log \frac{Q^2}{t_0}$ power in particular, are generated by the double poles in the r.h.s. of Eq. (2.6) which arise from the combination of the poles of $\Gamma(1-s)$ with the simple poles of $\mathcal{M}^{\text{HVP}}(s)$. As we shall see, it is because of the presence of non-analytic terms in this asymptotic expansion (terms with $k \geq 1$), that a specific transfer theorem is of relevance to HVP.

2.1 Conformal Mapping

The framework that we shall be using is the one which follows from performing a conformal mapping of the full complex q^2 -plane onto the unit disc $|\omega| \leq 1$ via the transformation

$$i \frac{1+\omega}{1-\omega} = \sqrt{\frac{q^2}{t_0} - 1}. \quad (2.8)$$

This mapping, illustrated in Figure 1, relates the Euclidean Q^2 -variable to the conformal ω -variable as follows:

$$z \equiv \frac{Q^2}{t_0} = \frac{4\omega}{(1-\omega)^2} \quad \text{and} \quad \omega = \frac{\sqrt{1+z} - 1}{\sqrt{1+z} + 1}. \quad (2.9)$$

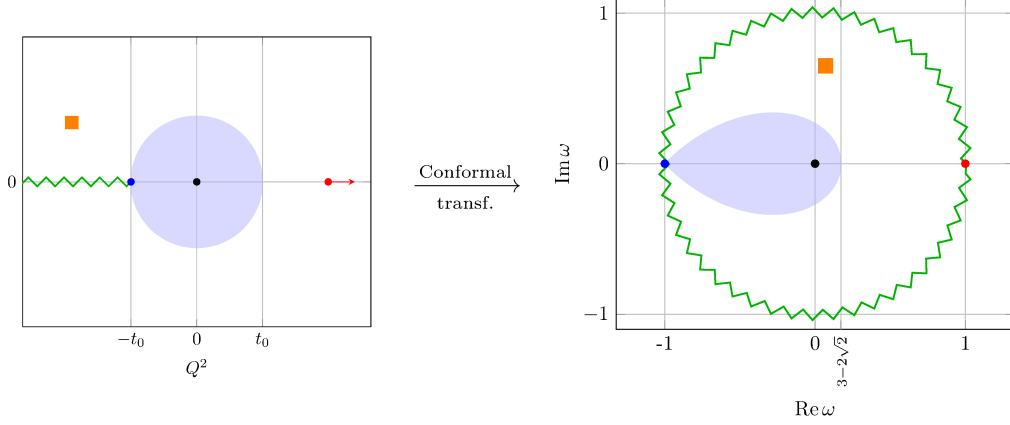


Figure 1. Conformal mapping of the Q^2 -plane in the left into the ω -plane at the right. The green zigzag lines correspond to the branching cut $\frac{Q^2}{t_0} < -1$. The black dot represents the $Q^2 = 0$ point on the left, mapped to $\omega = 0$ on the right. The blue dot corresponds to the physical threshold: $Q^2 = -t_0$ on the left mapped to $\omega = -1$ on the right. The red dot is the limit $Q^2 \rightarrow \infty$ on the left mapped to $\omega = 1$ on the right. The zones in blue are the regions where $|Q^2| \leq t_0$ in the Taylor expansion of $\Pi(Q^2)$: the disc on the left is mapped to the blue domain in the ω -variable. The orange square shows how an arbitrary point in the complex Q^2 -plane is transformed in the ω -plane.

Under this change of variables, the Taylor series in the r.h.s. of Eq. (2.4), becomes a power series in terms of the dimensionless ω -variable:

$$\Pi^{\text{HVP}}(-Q^2) \mapsto \Pi^{\text{HVP}}\left(-\frac{4\omega}{(1-\omega)^2}\right) \Big|_{|\omega|<1} \sim \sum_{n=1}^{\infty} \Omega_n \omega^n = \sum_{n=1}^{\infty} \Omega_n \left(\frac{\sqrt{1+\frac{Q^2}{t_0}} - 1}{\sqrt{1+\frac{Q^2}{t_0}} + 1} \right)^n, \quad (2.10)$$

with coefficients Ω_n ⁶ that are linear combinations of the Mellin moments in Eq. (2.5):

$$\Omega_n = \sum_{p=1}^n (-1)^p 4^p \frac{\Gamma(n+p)}{\Gamma(2p) \Gamma(n+1-p)} \mathcal{M}^{\text{HVP}}(1-p), \quad (2.11)$$

and reciprocally

$$\mathcal{M}^{\text{HVP}}(-n) = \frac{\Gamma(1+n) \Gamma(\frac{3}{2}+n)}{\sqrt{\pi}} \sum_{k=1}^{n+1} \frac{(-1)^k k}{\Gamma(2+n-k) \Gamma(2+n+k)} \Omega_k. \quad (2.12)$$

On the other hand, the conformal mapping of the asymptotic expansion in Eq. (2.7) when $Q^2 \rightarrow \infty$, results then in an asymptotic expansion for $\omega \rightarrow 1$:

$$\Pi^{\text{HVP}}\left(-\frac{4\omega}{(1-\omega)^2}\right) \Big|_{\omega \rightarrow 1} \sim \sum_{p=1,2,3,\dots} \sum_{k=0,1,2,\dots} \frac{(-1)^k}{k!} \mathcal{R}_{p,k} \left(\frac{(1-\omega)^2}{4\omega} \right)^{p-1} \log^k \frac{4\omega}{(1-\omega)^2}, \quad (2.13)$$

⁶One advantage of expressing $\Pi^{\text{HVP}}(-Q^2)$ as a power series in ω is that it increases considerably the rate of convergence. Both series in $\frac{Q^2}{t_0}$ -powers and in ω -powers converge to the same function; however, with the same number of terms in their expansions, the precision is better if one uses the series in ω rather than the series in $\frac{Q^2}{t_0}$.

and the transfer theorem becomes relevant because of the non-analytic $k \neq 0$ terms of this series.

2.2 The Imaginary Part

The terms of the Taylor series in Eq. (2.10) have imaginary parts which can be obtained by analytic continuation taking the following steps:

1. First observe that the second degree equation in ω in Eq. (2.9) has a discriminant

$$\Delta \equiv 16(1+z), \quad \text{where} \quad z \equiv \frac{Q^2}{t_0}. \quad (2.14)$$

2. For $z > -1$ one has $\Delta > 0$ and we get two solutions for ω :

$$\omega_+ = \frac{\sqrt{1+z}-1}{\sqrt{1+z}+1} \quad \text{and} \quad \omega_- = \frac{\sqrt{1+z}+1}{\sqrt{1+z}-1}. \quad (2.15)$$

The solution $\omega \equiv \omega_+$ is the one in Eq. (2.9), which we chose because it keeps the equivalence of the limits $Q^2 \rightarrow 0$ and $\omega \rightarrow 0$.

3. For $z < -1$ one has $\Delta < 0$, and in this case it is convenient to introduce the energy-momentum squared variable τ :

$$\tau \equiv -z = \left(-\frac{Q^2}{t_0}\right) \quad \text{with} \quad \tau \equiv \frac{t}{t_0} \geq 1. \quad (2.16)$$

The analytic continuation of the $\omega \equiv \omega_+$ solution is then

$$\frac{i\sqrt{\tau-1}+1}{i\sqrt{\tau-1}-1}. \quad (2.17)$$

4. We therefore have a twofold representation for the conformal ω -variable, either in terms of Q^2 or in terms of τ :

$$\omega = \begin{cases} \frac{\sqrt{1+\frac{Q^2}{t_0}}-1}{\sqrt{1+\frac{Q^2}{t_0}}+1} & \text{when } \frac{Q^2}{t_0} > -1, \\ \frac{i\sqrt{\tau-1}+1}{i\sqrt{\tau-1}-1} \equiv e^{-i\varphi} & \text{when } \frac{Q^2}{t_0} = -\tau \leq -1, \end{cases} \quad (2.18)$$

with the phase φ related to the τ -variable as follows ⁷:

$$\varphi = 2 \arctan \left(\frac{\text{Im } \omega}{\text{Re } \omega + |\omega|} \right) = 2 \arctan \left(\frac{1}{\sqrt{\tau-1}} \right) = \pi - 2 \arctan (\sqrt{\tau-1}). \quad (2.19)$$

Then

$$\sin \varphi = \frac{2\sqrt{\tau-1}}{\tau} \quad \text{and} \quad \cos \varphi = \frac{\tau-2}{\tau}. \quad (2.20)$$

⁷This determination takes into account the fact that the real part of ω (i.e. $\cos \varphi$) can be positive or negative.

5. For $|\omega| = 1$, the series in Eq.(2.10) generates an imaginary part series:

$$\sum_{n=1}^{\infty} \Omega_n \operatorname{Im}(\omega^n) = - \sum_{n=1}^{\infty} \Omega_n \sin(n\varphi) \quad (2.21)$$

which, in terms of the physical τ -variable, becomes a spectral function series:

$$\operatorname{Im}\Pi^{\text{HVP}}\left(\tau \equiv \frac{t}{t_0}\right) = - \sum_{n=1}^{\infty} \Omega_n \sin(n\varphi) = - \sum_{n=1}^{\infty} \Omega_n \sin \varphi \operatorname{U}_{n-1}(\cos \varphi) \quad (2.22)$$

$$= - \sum_{n=1}^{\infty} \Omega_n \frac{2\sqrt{\tau-1}}{\tau} \operatorname{U}_{n-1}\left(\frac{\tau-2}{\tau}\right), \quad (2.23)$$

where $\operatorname{U}_{n-1}(\cos \varphi)$ are Chebyshev polynomials of the second kind.

In QCD, the shape of the spectral function at threshold is fixed by lowest order chiral perturbation theory (χ PT):

$$\frac{1}{\pi} \operatorname{Im}\Pi^{\text{HVP}}\left(\tau \equiv \frac{t}{t_0}\right) \underset{\tau \rightarrow 1}{=} \frac{\alpha}{\pi} \frac{1}{12} (\tau-1)^{\frac{3}{2}} + \mathcal{O}\left[(\tau-1)^{\frac{5}{2}}\right]; \quad (2.24)$$

however, the behaviour at $\tau \rightarrow 1$ which follows from the expansion:

$$\sin(n\varphi) \underset{\tau \rightarrow 1}{=} -2n(-1)^n \sqrt{\tau-1} + \frac{2}{3} n(1+2n^2)(-1)^n (\tau-1)^{\frac{3}{2}} + \mathcal{O}\left[(\tau-1)^{\frac{5}{2}}\right] \quad (2.25)$$

in Eq. (2.22), results in a threshold behaviour:

$$\begin{aligned} \frac{1}{\pi} \operatorname{Im}\Pi^{\text{HVP}}\left(\tau \equiv \frac{t}{t_0}\right) \underset{\tau \rightarrow 1}{=} & \left[\frac{2}{\pi} \sum_{n=1}^{\infty} \Omega_n n (-1)^n \right] \sqrt{\tau-1} \\ & + \left[-\frac{2}{3\pi} \sum_{n=1}^{\infty} \Omega_n n (1+2n^2)(-1)^n \right] (\tau-1)^{\frac{3}{2}} + \mathcal{O}\left[(\tau-1)^{\frac{5}{2}}\right]. \end{aligned} \quad (2.26)$$

For consistency with χ PT, this requires two constraints on the Ω_n -coefficients:

$$\sum_{n=1}^{\infty} \Omega_n n (-1)^n = 0 \quad \text{and} \quad -\frac{4}{3\pi} \sum_{n=1}^{\infty} \Omega_n n^3 (-1)^n = \frac{\alpha}{\pi} \frac{1}{12} |F(t_0)|^2, \quad (2.27)$$

where $F(t_0)$ denotes the value of the electromagnetic pion form factor at threshold, which encodes the full hadronic correction to the lowest order χ PT result where $F(t_0) = 1$. We shall later explain how to include these two constraints in practice.

On the other hand, the spectral function in QCD when $\tau \rightarrow \infty$ is fixed by the asymptotic freedom limit:

$$\frac{1}{\pi} \operatorname{Im}\Pi^{\text{HVP}}\left(\tau \equiv \frac{t}{t_0}\right) \underset{\tau \rightarrow \infty}{\sim} \frac{\alpha}{\pi} \frac{N_c}{3} \sum_{\text{quarks}} e_q^2. \quad (2.28)$$

The series in Eq. (2.23), however, does not reproduce this property because for a fixed n -term

$$U_{n-1} \left(\frac{\tau-2}{\tau} \right) \underset{\tau \rightarrow \infty}{\sim} n - \frac{2}{3}n(n^2-1)\frac{1}{\tau} + \mathcal{O} \left(\frac{1}{\tau^2} \right). \quad (2.29)$$

This is an indication that the formal series in Eq. (2.23) must be a divergent series, which is precisely the point that brings us to the relevance of the transfer theorem discussed in the next section.

3 Reconstruction Approximants of the HVP Function

The transfer theorems of Flajolet and Odlyzko [20, 21] relate the non-analyticity of a given function defined in the unit ω -disc, to the large order coefficients of its Taylor expansion. As already mentioned, in the case of the HVP self-energy, the non-analyticity originates in the $\log^k(1-\omega)$ -terms of the asymptotic series in Eq (2.13). For the $k = 1$ terms in particular:

$$\sum_{p=1,2,3,\dots} (-2 \mathcal{R}_{p,1}) 4^{1-p} \left(\frac{(1-\omega)^2}{4\omega} \right)^{p-1} \log \left(\frac{1}{1-\omega} \right) \\ \underset{\omega \rightarrow 1}{=} \sum_{m=0,1,2,\dots} \tilde{\mathcal{R}}_{m,1} (1-\omega)^m \log \left(\frac{1}{1-\omega} \right), \quad (3.1)$$

with coefficients $\tilde{\mathcal{R}}_{m,1}$ that are linear combinations of the $\mathcal{R}_{p,1}$ residues

$$\tilde{\mathcal{R}}_{0,1} = -2\mathcal{R}_{1,1} \quad \text{and} \quad \tilde{\mathcal{R}}_{m,1} = -2 \sum_{p=2}^{\lfloor \frac{m+2}{2} \rfloor} \binom{m-p}{p-2} 4^{1-p} \mathcal{R}_{p,1} \quad \text{for } m \geq 1, \quad (3.2)$$

and in the pQCD asymptotic freedom limit

$$\tilde{\mathcal{R}}_{0,1} = -2\mathcal{R}_{1,1} = -2 \frac{\alpha}{\pi} \frac{N_c}{3} \left(\sum_{\text{quarks}} e_q^2 \right). \quad (3.3)$$

The appropriate transfer theorem in this case ⁸ states that the behaviour of the Ω_n coefficients of the Taylor series

$$\Pi^{\text{HVP}} \left(-\frac{4\omega}{(1-\omega)^2} \right) \underset{|\omega|<1}{\sim} \sum_{n>0} \Omega_n \omega^n, \quad (3.4)$$

at their large- n values, must be of the form

$$\Omega_n \underset{n \rightarrow \infty}{\sim} \Omega_n^{\text{AS}} = \sum_{j=0}^{\infty} \sum_{m=0}^{\infty} \tilde{\mathcal{R}}_{m,1} \left\{ \begin{matrix} m+j \\ m \end{matrix} \right\} \frac{(-1)^m \Gamma(m+1)}{n^{m+j+1}}, \quad (3.5)$$

⁸See Appendix B for a proof, where the general case for $k \geq 1$ is also discussed.

where $\begin{Bmatrix} a \\ b \end{Bmatrix}$ are Stirling numbers of the second kind [27].

The *reconstruction approximants* of the HVP self-energy function consists then in replacing the infinite sums in the identity:

$$\Pi^{\text{HVP}} \left(-\frac{4\omega}{(1-\omega)^2} \right) = \sum_{n=1}^{\infty} (\Omega_n - \Omega_n^{\text{AS}}) \omega^n + \sum_{n=1}^{\infty} \Omega_n^{\text{AS}} \omega^n, \quad (3.6)$$

by successive N,L-functions:

$$\Pi_{\text{N,L}}^{\text{HVP}} \left(-\frac{4\omega}{(1-\omega)^2} \right) \doteq \sum_{n=1}^{\text{N}} (\Omega_n - \Omega_{n,\text{L}}^{\text{AS}}) \omega^n + \sum_{n=1}^{\infty} \Omega_{n,\text{L}}^{\text{AS}}(\omega), \quad (3.7)$$

with $\sum_{n=1}^{\infty} \Omega_{n,\text{L}}^{\text{AS}}(\omega)$ evaluated in terms of a finite sum of polylog $\text{Li}_l(\omega)$ functions with $1 \leq l \leq \text{L}$. These polylogs result from applying their definition:

$$\text{Li}_l(\omega) = \sum_{n=1}^{\infty} \frac{\omega^n}{n^l}, \quad \text{Li}_l(\omega) = \int_0^\omega \frac{d\omega}{\omega} \text{Li}_{l-1}(\omega), \quad \text{Li}_1(\omega) = -\log(1-\omega), \quad |\omega| \leq 1, \quad (3.8)$$

to the power factors $\frac{1}{n^{m+j+1}}$ in the asymptotic Ω_n^{AS} series in Eq. (3.5). Setting $m+j+1 \doteq l$, we have

$$\sum_{n=1}^{\infty} \Omega_{n,\text{L}}^{\text{AS}}(\omega) = \sum_{l=1}^{\text{L}} \mathcal{B}_l \sum_{n=1}^{\infty} \frac{\omega^n}{n^l} = \sum_{l=1}^{\text{L}} \mathcal{B}_l \text{Li}_l(\omega) \quad (3.9)$$

where, as shown in the Appendix B, the \mathcal{B}_l -coefficients are linear combinations of the $\tilde{\mathcal{R}}_{m,1}$ -coefficients in Eq. (3.2) and hence, linear combinations of the residues $\mathcal{R}_{p,1}$:

$$\mathcal{B}_1 = -2\mathcal{R}_{1,1} \text{ and } \mathcal{B}_l = \sum_{m=1}^{l-1} \tilde{\mathcal{R}}_{m,1} \begin{Bmatrix} l-1 \\ m \end{Bmatrix} (-1)^m \Gamma(m+1) \quad \text{with } \mathcal{B}_{l \text{ even}} = 0. \quad (3.10)$$

The successive *reconstruction approximants* in Eq. (3.7) are thus defined by partial N and L sums:

$$\Pi_{\text{N,L}}^{\text{HVP}} \left(-\frac{4\omega}{(1-\omega)^2} \right) \doteq \sum_{n=1}^{\text{N}} \underbrace{(\Omega_n - \Omega_{n,\text{L}}^{\text{AS}})}_{\mathcal{A}(n,\text{L})} \omega^n + \sum_{l=1}^{\text{L}} \mathcal{B}_l \text{Li}_l(\omega), \quad (3.11)$$

with the $\mathcal{A}(n,\text{L})$ and \mathcal{B}_l parameters of the approximation to be fixed either from the Mellin transform of the spectral function of the underlying theory, as illustrated with the QED example in Appendix I, or as in the case of the MUonE proposal, from a fit to the data values of the experimental determination of the HVP self-energy function. As the number of N terms increases and the number L of polylog functions increases, the $\Pi_{\text{N,L}}^{\text{HVP}} \left(-\frac{4\omega}{(1-\omega)^2} \right)$ approximants reconstruct better and better the wanted $\Pi^{\text{HVP}} \left(-\frac{4\omega}{(1-\omega)^2} \right)$ function.

We shall later discuss how to attribute a systematic error to a fixed $\Pi_{N,L}^{\text{HVP}}(\dots)$ approximant, hence, to its contribution to a_μ^{HVP} .

As compared to other procedures discussed in the literature, the method of *reconstruction approximants*, only uses information provided by the experimental determination of the HVP self-energy in a specific set of values of its argument. It does not require extra input from other sources, like LQCD and/or phenomenological models. This offers, therefore, an opportunity for a future MUonE experiment to provide a completely independent determination of a_μ^{HVP} .

3.1 Approximants from Asymptotic Freedom

The simplest examples of *reconstruction approximants* of the HVP self-energy function are the ones with $L=1$ and a few N terms.

In QCD, the leading singular behaviour of the function $\Pi^{\text{HVP}}(-Q^2)$ at large- Q^2 is governed by the first pole at $s = 1$ in the singular series of Eq. (3.5), with a residue $\mathcal{R}_{1,1}$ known from the asymptotic freedom limit behaviour:

$$\Pi^{\text{HVP}}(-Q^2) \underset{Q^2 \rightarrow \infty}{\sim} -\mathcal{R}_{1,1} \log\left(\frac{Q^2}{t_0}\right), \quad \text{and} \quad \mathcal{R}_{1,1} = \frac{\alpha}{\pi} \frac{N_c}{3} \left(\sum_{\text{quarks}} e_q^2 \right). \quad (3.12)$$

There are corrections to this limit generated by the $\alpha_{\text{QCD}}(Q^2)$ power series of pQCD. We shall not include them here although, if necessary, they could also be taken into account using the results discussed in Appendix B.

In the conformal ω -disc, asymptotic freedom produces the non-analytic term:

$$\Pi^{\text{HVP}}\left(-\frac{4\omega}{(1-\omega)^2}\right) \underset{\omega \rightarrow 1}{\sim} -2 \mathcal{R}_{1,1} \log\left(\frac{1}{1-\omega}\right) \quad (3.13)$$

and therefore, according to Eqs. (3.5) and (3.11),

$$\Omega_n \underset{n \rightarrow \infty}{\sim} \Omega_n^{\text{AS}} = -2 \mathcal{R}_{1,1} \frac{1}{n} \quad \text{and} \quad \mathcal{A}(n, 1) \equiv \Omega_n + 2 \mathcal{R}_{1,1} \frac{1}{n}. \quad (3.14)$$

In this case, the *reconstruction approximants* of Eq. (3.11) are rather simple. They consist in evaluating the successive N -sums:

$$\Pi_{N,1}^{\text{HVP}}(-Q^2) = \sum_{n=1}^N \mathcal{A}(n, 1) \left(\frac{\sqrt{1 + \frac{Q^2}{t_0}} - 1}{\sqrt{1 + \frac{Q^2}{t_0}} + 1} \right)^n + 2 \mathcal{R}_{1,1} \log\left(1 - \frac{\sqrt{1 + \frac{Q^2}{t_0}} - 1}{\sqrt{1 + \frac{Q^2}{t_0}} + 1}\right), \quad (3.15)$$

with only one reconstruction term which in this case is the leading polylog $\text{Li}_1(\omega) = -\log(1 - \omega)$ function.

The application of this result to the MUonE-experiment consists then in using the sum of functions above as a “first set of approximants” to the full integrand in the r.h.s. of Eq. (1.10). More precisely, the *reconstruction approximants* in this case are:

$$(1-x) \Pi_{N,1}^{\text{HVP}} \left(-\frac{x^2}{1-x} m_\mu^2 \right) \doteq (1-x) \left\{ \sum_{n=1}^N \mathcal{A}(n,1) \left(\frac{\sqrt{1 + \frac{x^2}{1-x} \frac{m_\mu^2}{t_0}} - 1}{\sqrt{1 + \frac{x^2}{1-x} \frac{m_\mu^2}{t_0}} + 1} \right)^n + 2 \mathcal{R}_{1,1} \log \left(1 - \frac{\sqrt{1 + \frac{x^2}{1-x} \frac{m_\mu^2}{t_0}} - 1}{\sqrt{1 + \frac{x^2}{1-x} \frac{m_\mu^2}{t_0}} + 1} \right) \right\}, \quad (3.16)$$

with unknown coefficients $\mathcal{A}(n,1)$, which are free parameters to be fixed from a linear fit to the experimental data in the x -window where the quality of the data is best. Using the values of the $\mathcal{A}(n,1)$ parameters thus obtained, Eq. (1.10) provides then the way to obtain the corresponding approximate evaluations of the HVP contribution to the muon anomaly.

As discussed before, the approximants in Eq. (3.15) have imaginary parts which give corresponding “effective spectral series approximants”. The power terms in Eq. (3.16) generate imaginary parts similar to those given in Eq. (2.23) except that now the series are from $n = 1$ to a finite N -value and the $\mathcal{A}(n,1)$ coefficients now replace the Ω_n . The imaginary part of the logarithmic term in Eq. (3.16) gives

$$\text{Im} [\log(1 - \omega)] = \text{Im} \left[\log \left(\frac{2}{\tau} - i \frac{2\sqrt{\tau-1}}{\tau} \right) \right] = -\arctan(\sqrt{\tau-1}), \quad (3.17)$$

and therefore, the “effective spectral functions” associated to the approximants $\Pi_{N,1}^{\text{HVP}}(-Q^2)$ in Eq. (3.15) are then given by the N -sums (recall that $\tau = \frac{t}{t_0}$):

$$\frac{1}{\pi} \text{Im} \Pi_{N,1}^{\text{HVP}}(t) = \frac{2}{\pi} \left\{ -\frac{\sqrt{\tau-1}}{\tau} \sum_{n=1}^N \mathcal{A}(n,1) U_{n-1} \left(\frac{\tau-2}{\tau} \right) + \mathcal{R}_{1,1} \arctan(\sqrt{\tau-1}) \right\} \theta(\tau-1). \quad (3.18)$$

To this, one can also apply the constraints in Eq. (2.27) which can be easily adapted to the threshold expansion of the r.h.s. of Eq. (3.18) i.e. ⁹

$$0 = \sum_{n=1}^N \mathcal{A}(n,1) n (-1)^n + \mathcal{R}_{1,1} \quad \text{and} \quad \frac{\alpha}{\pi} \frac{1}{12} |F(t_0)|^2 = -\frac{4}{3\pi} \sum_{n=1}^N \mathcal{A}(n,1) n^3 (-1)^n, \quad N \geq 2. \quad (3.19)$$

3.2 Asymptotic freedom and Lowest Order χ PT

The case $L=1$ with $N=2$ is particularly interesting because, quite remarkably, the parameters $\mathcal{A}(1,1)$ and $\mathcal{A}(2,1)$ can then be fixed from asymptotic freedom and lowest order χ PT alone. In this case, the two constraints in Eq. (3.19), with $F(t_0) = 1$, result in the values (in $\frac{\alpha}{\pi}$ units)

$$\mathcal{A}(1,1) = 2.156 \dots \quad \text{and} \quad \mathcal{A}(2,1) = 0.2450 \dots, \quad (3.20)$$

and the shape of the muon anomaly integrand for these values is the one shown in Fig. (2).

⁹It is not necessary to fix the value of $F(t_0)$ from phenomenology. It can also be taken as a free parameter in the fit.

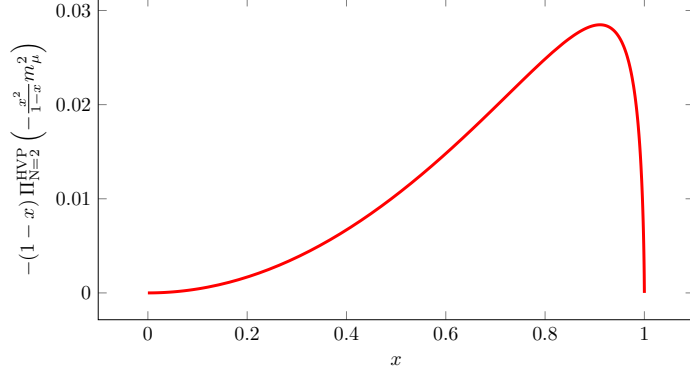


Figure 2. Shape of the x -integrand in Eq. (1.10) in $\frac{\alpha}{\pi}$ units, corresponding to the reconstruction approximant: $N = 2$, $L = 1$.

The resulting value for the HVP contribution to the muon anomaly is

$$a_{\mu}^{\text{HVP}} \Big|_{N=2} = (6527.12 \dots) \times 10^{-11}, \quad (3.21)$$

which reproduces the center value of the dispersive data -driven evaluations in Eq. (1.5) at the 6% level (quite encouraging¹⁰). We wish to emphasize the fact that only two rigorous limits of QCD have been used to obtain this result: the short-distance asymptotic freedom limit and the long-distance lowest order χ PT limit.

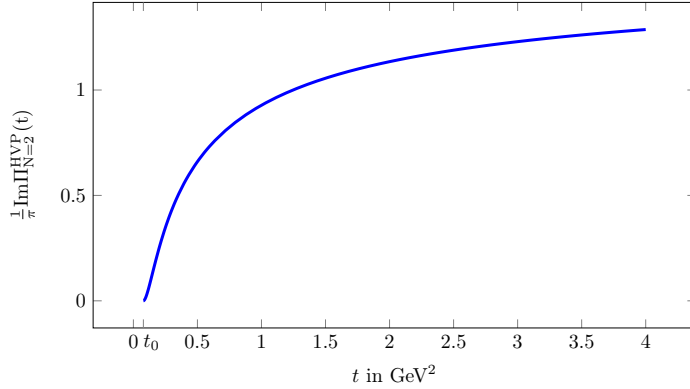


Figure 3. Shape of the spectral function for $N = 2$ in $\frac{\alpha}{\pi}$ units.

The shape of the “effective spectral function” in Eq. (3.18) associated to the $\Pi_{N=2}^{\text{HVP}}(-Q^2)$ approximant in Fig. (2) is shown in Fig. (3). We insist on the fact that, contrary to the Euclidean shape in Fig. (2) which is expected to be a local approximation at each x -value, the corresponding “effective spectral function” is not a locally dual approximation at a fixed t -value of the physical spectrum. Only moments and/or weighted integrals of this “effec-

¹⁰Not yet the accuracy that one wants of course, but already better than some of the LQCD evaluations.

tive spectral function” can be considered as good approximants¹¹. However, as more and more N-power terms and L-polylog functions are taken into account in the reconstruction approximants of Eq. (3.11), the corresponding ”effective spectral functions” are expected to become more and more locally dual to the physical spectral function.

The reason why we only consider the functions in Eq. (3.15) as a ”first set” of *reconstruction approximants*, is because they only include the non-analyticity in the conformal ω -domain associated to asymptotic freedom, i.e. the leading $s = 1$ singularity of the hadronic Mellin transform. In the next section we shall show how to construct *reconstruction approximants*, adapted to the MUonE-experiment, when one also includes higher order singularities.

4 Reconstruction Approximants for the MUonE Proposal

In the QED example discussed in Appendix A, there is only one mass scale, the fermion mass M . The singular pattern of the two-point function is therefore rather simple. In the case of the electromagnetic interactions of hadrons, one obviously expects to have more underlying mass scales and, therefore, a more complicated singular pattern. In fact, in QCD, the operator product expansion (OPE) applied to $\Pi^{\text{HVP}}(-Q^2)$ shows the existence of other mass scales than quark masses. They appear as vacuum expectation values of local colour singlet operators [28], like e.g. the gluon condensate. A possible option could have been to apply the transfer theorem method using the OPE contributions as an input. These OPE contributions, however, are poorly known both from phenomenology and theory where the separation of perturbative and non-perturbative scales is problematic¹². Concerning the application to the MuonE experiment, we are therefore more inclined to apply the *reconstruction approximants* defined in Eq. (3.11), using input from experiment alone. More precisely, in units of $\frac{\alpha}{\pi}$, the approximants to be considered for the integrand in the Feynman- x representation given in Eq. (1.10) are:

$$-(1-x) \Pi_{\text{N,L}}^{\text{HVP}} \left(-\frac{x^2}{1-x} m_\mu^2 \right) = -(1-x) \left\{ \sum_{n=1}^N \mathcal{A}(n, L) \left(\frac{\sqrt{1+\frac{x^2}{1-x} \frac{m_\mu^2}{t_0}} - 1}{\sqrt{1+\frac{x^2}{1-x} \frac{m_\mu^2}{t_0}} + 1} \right)^n + \sum_{p=1}^{\lfloor \frac{L+1}{2} \rfloor} \mathcal{B}(2p-1) \text{Li}_{2p-1} \left(\frac{\sqrt{1+\frac{x^2}{1-x} \frac{m_\mu^2}{t_0}} - 1}{\sqrt{1+\frac{x^2}{1-x} \frac{m_\mu^2}{t_0}} + 1} \right) \right\}, \quad (4.1)$$

where the terms in the second line, similarly to the QED example discussed in Appendix A, correspond to the Polylog series of Eq. (3.11). However, contrary to the QED example where the coefficients $\mathcal{A}(n, L)$ and $\mathcal{B}(2p-1)$ are fixed by the theory, they are here free parameters, to be fixed from a linear fit of the functional approximants to the experimental data in the x -window where the quality of the data is best.

¹¹The dispersive representation in Eq. (1.9) is a weighted integral of the spectral function and the result which follows from inserting the “N=2 effective spectral function” in this representation gives, as expected, the same value as the one in Eq. (3.21) using the Euclidean representation.

¹²For a recent discussion, where earlier references can also be found, see e.g. ref [29].

We finally comment on a technical simplification that we have made in the derivation of the *reconstruction approximants* above: the fact that we have restricted the singular behaviour of the Mellin transform of the physical hadronic spectral function to poles of multiplicity one at most. In other words, the non-analytic terms generated by the singular series in Eq. (2.7) has been limited to terms with $k = 1$, which corresponds to terms with one power of $\log Q^2$ at most in the large- Q^2 expansion. As shown in Appendix B, it is possible to generalize the *reconstruction approximants* so as to include the effect of $k > 1$ terms; but this is at the expense of introducing more parameters and extra derivatives of the Li_{2p-1} functions. Because of the complexity involved, we have not considered this generalization in this paper. It is reassuring, however, to know that the assumption of simple poles in the Mellin transform is certainly satisfied, not only in QED, but also in many phenomenological models of the hadronic spectral function; in particular for superpositions of Breit-Wigner-like terms. In all these cases, the transfer theorem guaranties that, as the number of N-terms and polylog L-like terms in Eq. (4.1) increases, with more and more data points used in the fits of the $\mathcal{A}(n, L)$ and $\mathcal{B}(2p-1)$ parameters, the approximants converge to the physical Euclidean-integrand in its full range.

As in the QED example discussed in Appendix A, the approximants in Eq. (4.1) have imaginary parts that can be interpreted as “effective spectral function approximants” associated to the corresponding Euclidean approximants. They can be evaluated following the same steps as in the QED example, with the result ($\tau = \frac{t}{t_0}$):

$$\begin{aligned} \frac{1}{\pi} \text{Im} \Pi_{N,L}^{\text{HVP}}(\tau) &= \frac{\alpha}{\pi} \left\{ -\frac{1}{\pi} \frac{2\sqrt{\tau-1}}{\tau} \sum_{n=1}^N \mathcal{A}(n, L) U_{n-1} \left(1 - \frac{2}{\tau} \right) \right. \\ &\quad \left. + \sum_{p=1}^{\lfloor \frac{L+1}{2} \rfloor} \mathcal{B}(2p-1) B_{2p-1} \left(\frac{\pi - 2 \arctan(\sqrt{\tau-1})}{2\pi} \right) \right\} \theta(\tau-1), \end{aligned} \quad (4.2)$$

where $B_{2p-1}(\dots)$ are Bernoulli polynomials. As already mentioned, these “effective spectral function approximants” are only globally dual to the physical spectral function. Only their moments are to be considered as good approximants to the physical moments. When introduced in the dispersive integral representation in Eq. (1.9), which is a weighted integral of the spectral function, they reproduce the same values for the anomaly as those resulting from the Euclidean integration of the $\Pi_{N,L}^{\text{HVP}} \left(-\frac{x^2}{1-x} m_\mu^2 \right)$ approximants in Eq. (1.10).

The threshold constraints discussed earlier in Eqs. (2.27) and (3.19), when adapted to the threshold expansion of the r.h.s. in Eq. (4.2), and keeping terms up to $L=5$, are:

$$0 = \sum_{n=1}^{\infty} \mathcal{A}(n, 5) n (-1)^n + \frac{5}{3} - \frac{\pi^2}{12} \mathcal{B}(3) - \frac{7\pi^4}{720} \mathcal{B}(5), \quad (4.3)$$

and

$$-\frac{3\pi}{4} \chi_{\frac{3}{2}} = \sum_{n=1}^{\infty} \mathcal{A}(n, 5) (-1)^n n^3 - \frac{1}{2} \mathcal{B}(3) - \frac{\pi^2}{12} \mathcal{B}(5), \quad (4.4)$$

where as in Eq. (3.19) $\chi_{\frac{3}{2}} \equiv \frac{\alpha}{\pi} \frac{1}{12} |F(t_0)|^2$; but $\chi_{\frac{3}{2}}$ can also be taken as a free parameter in the fit.

The systematic errors of the *reconstruction approximants* in Eq. (4.1) are given by the terms not included in the finite sums which define a specific approximant i.e., for a fixed L , the systematic error $\mathcal{E}_{N,L}(\omega)$ is:

$$\mathcal{E}_{N,L}(\omega) = \sum_{n=N+1}^{\infty} \mathcal{A}(n, L) \omega^n, \quad (4.5)$$

with the $\mathcal{A}(n, L)$ coefficients restricted by the transfer theorem to behave as

$$\mathcal{A}(n, L) \underset{n \rightarrow \infty}{=} \mathcal{O}\left(\frac{1}{n^{L+1}}\right), \quad (4.6)$$

which implies that for n sufficiently large, say $n > N^*$, and \mathcal{C}_{N^*} a constant a priori unknown,

$$n^{L+1} |\mathcal{A}(n, L)| \underset{n > N^*}{<} \mathcal{C}_{N^*}. \quad (4.7)$$

This results in an upper bound for the systematic error

$$|\mathcal{E}_{N^*,L}(\omega)| \leq \left| \mathcal{C}_{N^*} \sum_{n=N^*+1}^{\infty} \frac{\omega^n}{n^{L+1}} \right| = \left| \mathcal{C}_{N^*} \omega^{N^*+1} \Phi(\omega, L+1, N^*+1) \right| \equiv \Delta_{\text{error}}(\omega, L, N^*, \mathcal{C}_{N^*}), \quad (4.8)$$

where $\Phi(\omega, L+1, N^*+1)$ is the Hurwitz-Lerch transcendental function. The propagation of this error in the integral which gives the HVP determination of a_{μ}^{HVP} , fixes then an upper bound to the systematic error of the anomaly evaluation:

$$\mathcal{E}[a_{\mu}^{\text{HVP}}]_{N^*,L} = \frac{\alpha}{\pi} \int_0^1 dx (1-x) \Delta_{\text{error}}(\omega, L, N^*, \mathcal{C}_{N^*}), \quad \text{with} \quad \omega = \frac{\sqrt{1 + \frac{x^2}{1-x} \frac{m_{\mu}^2}{t_0}} - 1}{\sqrt{1 + \frac{x^2}{1-x} \frac{m_{\mu}^2}{t_0}} + 1}. \quad (4.9)$$

It remains to be seen how to estimate in practice the values of the N^* and \mathcal{C}_{N^*} parameters, when the only information one has about the underlying dynamics is the one provided by the x -data points which have been used to fit the $\mathcal{A}(n, L)$ and $\mathcal{B}(2p-1)$ parameters of the approximant. In the next subsection, we illustrate the procedure to follow, with an example where the “data” are obtained from a simple phenomenological model of the hadronic spectral function.

5 Illustration with a Phenomenological Model

The spectral function of the model we have adopted is inspired from χ PT and phenomenology¹³:

¹³It is a simplified version of phenomenological spectral functions discussed in the literature, see e.g. refs. [30, 31] and references therein.

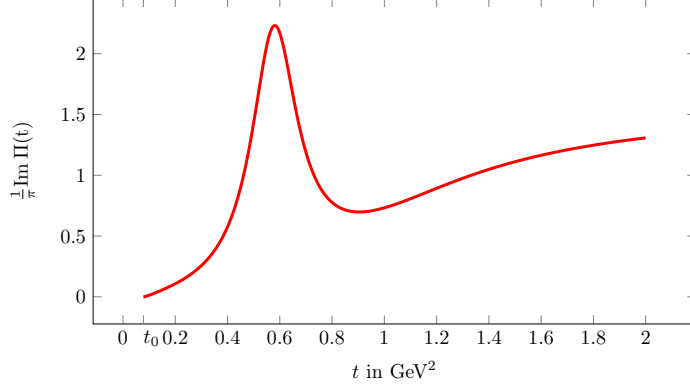


Figure 4. The model spectral function in Eq. (5.1) for $t_c = 1 \text{ GeV}^2$ and $\Delta = 0.5 \text{ GeV}^2$ in $\frac{\alpha}{\pi}$ -units.

$$\frac{1}{\pi} \text{Im} \Pi_{\text{model}}^{\text{HVP}}(t) = \frac{\alpha}{\pi} \left(1 - \frac{4m_\pi^2}{t}\right)^{3/2} \left\{ \frac{1}{12} |F(t)|^2 + \sum_{\text{quarks}} e_q^2 \Theta(t, t_c, \Delta) \right\} \theta(t - 4m_\pi^2). \quad (5.1)$$

It has a Breit-Wigner-like modulus squared form factor

$$|F(t)|^2 = \frac{M_\rho^4}{(M_\rho^2 - t)^2 + M_\rho^2 \Gamma(t)^2}, \quad (5.2)$$

with an energy dependent width:

$$\Gamma(t) = \frac{M_\rho t}{96\pi f_\pi^2} \left[\left(1 - \frac{4m_\pi^2}{t}\right)^{3/2} \theta(t - 4m_\pi^2) + \frac{1}{2} \left(1 - \frac{4M_k^2}{t}\right)^{3/2} \theta(t - 4M_k^2) \right]; \quad (5.3)$$

plus a function

$$\Theta(t, t_c, \Delta) = \frac{\frac{2}{\pi} \arctan\left(\frac{t-t_c}{\Delta}\right) - \frac{2}{\pi} \arctan\left(\frac{t_0-t_c}{\Delta}\right)}{1 - \frac{2}{\pi} \arctan\left(\frac{t_0-t_c}{\Delta}\right)}, \quad (5.4)$$

with two arbitrary parameters t_c and Δ . This function has been added so as to smoothly match the low energy phenomenological spectrum of the model to the pQCD asymptotic continuum generated by the sum of quark flavors. The shape of this spectral function, using the physical central values for m_π , M_k , M_ρ , $f_\pi = 93.3 \text{ MeV}$, and $t_c = 1 \text{ GeV}^2$, $\Delta = 0.5 \text{ GeV}^2$ with $\sum_{\text{quarks}} e_q^2 = \frac{5}{3}$, is shown in Fig (4).

The Euclidean self-energy function of the model with these parameters is given by the integral

$$\Pi_{\text{model}}(Q^2) \equiv - \int_{t_0}^{\infty} \frac{dt}{t} \frac{Q^2}{t + Q^2} \frac{1}{\pi} \text{Im} \Pi_{\text{model}}^{\text{HVP}}(t), \quad Q^2 \equiv \frac{x^2}{1-x} m_\mu^2. \quad (5.5)$$

It provides a model example to obtain “data” at different values of the Feynman x -variable. The contribution to the muon anomaly in this model is ¹⁴

$$a_\mu^{\text{HVP}}(\text{model}) = -\frac{\alpha}{\pi} \int_0^1 dx (1-x) \Pi_{\text{model}}\left(\frac{x^2}{1-x} m_\mu^2\right) = 6992.4 \times 10^{-11}, \quad (5.6)$$

¹⁴Only central values are used in the model illustration of this section.

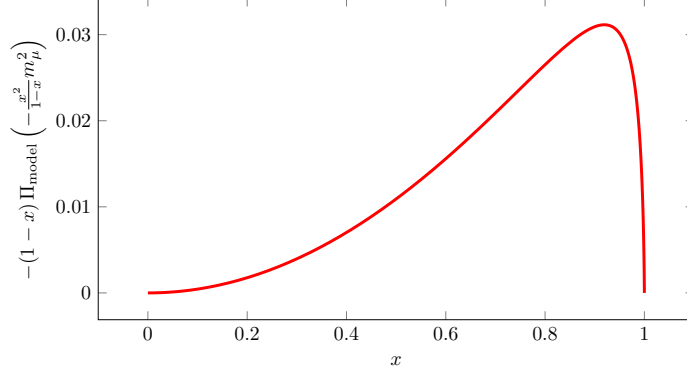


Figure 5. Plot of the Euclidean integrand in Eq. (5.6) for $t_c = 1 \text{ GeV}^2$ and $\Delta = 0.5 \text{ GeV}^2$ in $\frac{\alpha}{\pi}$ -units.

and the shape of the integrand is shown in Fig. (5).

We next propose to fix the values of the parameters $\mathcal{A}(n, L)$ and $\mathcal{B}(2p - 1)$ of the *reconstruction approximants* in Eq. (4.1), from a linear fit to “data-points” provided by the $\Pi_{\text{model}}(Q^2)$ function. We choose for that a set of x -points in the interval $0.23 \leq x \leq 0.93$ in fifty equal steps; a choice motivated by the x -region where the MUonE experiment expects to have the best quality of measurements [32]. We have used the Mathematica **nlm** code to do the linear fits, with the following results:

5.1 Approximants with L=1 only

These are the “first step approximants” that were introduced in Eq. (3.16). The results for $a_\mu^{\text{HVP}}(N)$, for a number of N terms with the function $L=1$, are the black dot points in Fig. (6) with an estimate, discussed below, of the systematic error bars included. The vertical scale in the figure corresponds to a choice of 0.1% accuracy, attributed to the model value of the anomaly represented by the horizontal red dashed line.

The estimate of the systematic error bars is based on the discussion at the end of Section IV (Eqs. (4.8) and (4.9) in particular):

i) For a fixed N , we choose $N^* = N + 1$ and the constant \mathcal{C}_{N^*} evaluated by the quadratic mean of the previously evaluated $\mathcal{A}(n, L = 1)$ coefficients:

$$\mathcal{C}_{N^*} \equiv \sum_{n=1}^N \frac{1}{N} \sqrt{|\mathcal{A}(n, L = 1)|^2}. \quad (5.7)$$

ii) The systematic error attributed to the evaluation of the anomaly $a_\mu^{\text{HVP}}(N)$ is then given by the integral in Eq. (4.9) with N^* and \mathcal{C}_{N^*} fixed as previously explained.

As shown in Fig. (6) (notice the vertical scale in the figure), for $N=4,5,\dots,10$ the results are very stable and reproduce the model value in Eq. (5.6), represented by the horizontal dashed red line, to an excellent accuracy. Beyond $N \sim 10$, the results become unstable and larger, which is an indication that there is a limit on the number of N -terms one can take in the *reconstruction approximants* when keeping only the leading $L=1$ function.

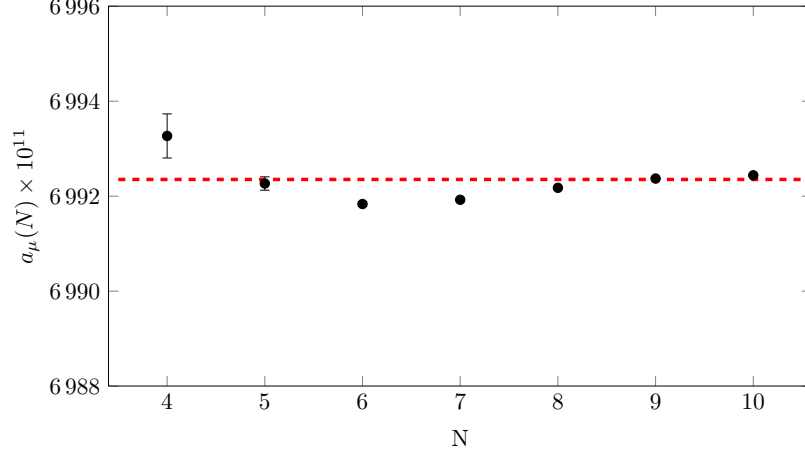


Figure 6. $a_\mu^{\text{HVP}}(N)$ results with estimated systematic error bars. The horizontal red dashed line is the a_μ^{HVP} value of the model.

5.2 Reconstruction Approximants with Threshold Constraints

The *reconstruction approximants* in this case are those in Eq. (4.1) where, for each fixed number of N -power terms, we add to the leading $L = 1$ function the contribution from the next two polylog functions with coefficients $\mathcal{B}(3)$ and $\mathcal{B}(5)$. The parameters to be fixed are then

$$\mathcal{A}(n, L) \quad \text{with } n = 1, 2, 3, \dots, L \leq 5 \quad \text{and} \quad \mathcal{B}(3), \mathcal{B}(5); \quad (5.8)$$

restricted by the threshold constraints in Eqs. (4.3) and (4.4). The two linear constraint equations can then be used to fix the $\mathcal{B}(3)$ and $\mathcal{B}(5)$ parameters in terms of the $\mathcal{A}(n, L)$ and $\chi_{\frac{3}{2}} \equiv \frac{\alpha}{\pi} \frac{1}{12} |F(t_0)|^2$, which are then left as free parameters for a fit to the data.

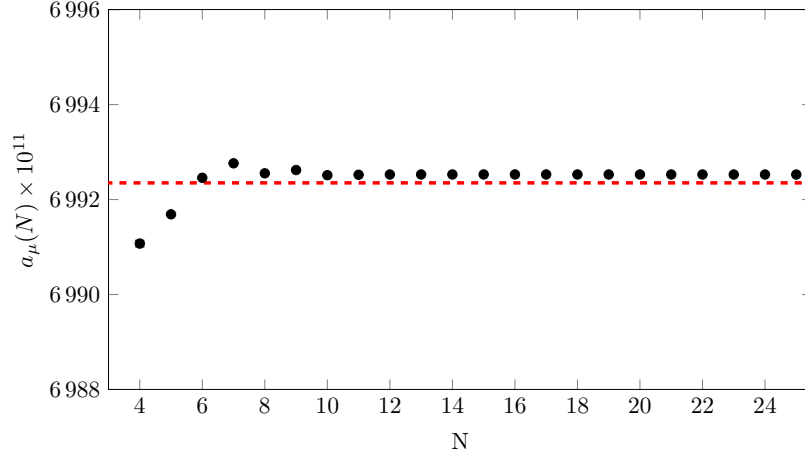


Figure 7. $a_\mu^{\text{HVP}}(N, L = 5)$ results with estimated systematic error bars. The horizontal red dashed line is the a_μ^{HVP} value of the model.

The results for $a_\mu^{\text{HVP}}(N, L = 5)$, for a number of N terms with three L -functions are the black dot points in Fig. (7). The estimated systematic error bars are given by $\Delta_{\text{error}}(\omega, L, N^*, \mathcal{C}_{N^*})$ in Eqs. (4.8) and (4.9), with the choice of \mathcal{C}_{N^*} the same as in Eq. (5.7) but for $L = 5$. The vertical scale is the same as in Fig. (6), which corresponds to a choice of 0.1% accuracy, attributed to the model value of the anomaly represented by the horizontal red dashed line. As shown in Fig. (7) the results remain, very accurate, and stable up to a very high number of terms.

As already discussed before, the *reconstruction approximants* have imaginary parts; in this case given by Eq. (4.2). They can be considered as “globally equivalent” spectral function approximants. Figure (8) shows, in blue, the shape of the “equivalent” spectral function approximant corresponding to the choice $N=20$. Although it is not “locally dual” to the model spectral function in red, its weighted integral using Eq. (1.9), reproduces the same value for $a_\mu^{\text{HVP}}(20, 5)$ as using the x -Feynman representation in Eq. (1.10).

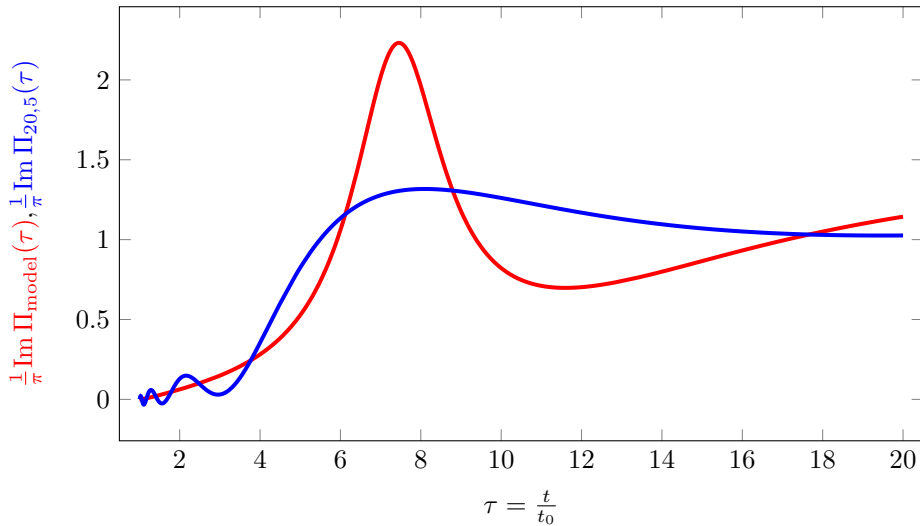


Figure 8. “Equivalent” spectral function approximant in blue, for $N=20$ and $L=5$. In red the model spectral function.

6 Conclusions and Outlook

We conclude that *Reconstruction Approximants*, based on the work of Flajolet and Odlyzko [20], provide an excellent way to extrapolate the determination of two-point functions in regions neither covered by model independent evaluations nor by precise enough experimental determinations. In the Appendix I, we have illustrated the underlying theory of reconstruction with the example of vacuum polarization in QED at the one loop level, where all the steps have been made analytically. Our main purpose, however, has been to show how to apply these approximants to extend the evaluations of the HVP self-energy to the

x -regions where the MUonE proposal will not have access with sufficient accuracy. We have illustrated how to do this in practice with the help of a phenomenological model. The results, shown in Figs. (6) and (7), are extremely encouraging. They don't include, however, the statistical errors of an experiment, neither the optimal choice of the data points to perform a fit. This is something beyond the scope of this paper.

Based on the work described above, we believe that the use of *reconstruction approximants* enhances the interest of the MUonE proposal as an independent and competitive way to measure a_μ^{HVP} . As compared to other methods suggested in the literature, *reconstruction approximants* don't require extra input from either phenomenological estimates or LQCD evaluations. This gives the possibility that a MUonE experiment [32, 33] may provide a totally independent result from either the dispersive evaluations in refs. [7, 8] or the LQCD determination of ref. [6].

We are aware of the fact that the *reconstruction approximants* proposed in this paper can also be applied to many other cases; in particular to the Euclidean representation of a_μ^{HVP} at next-to-leading order, recently discussed in ref. [34]. Any observable governed by integrals of two-point functions is a possible candidate.

The time momentum representation proposed in ref. [35] for LQCD evaluations of a_μ^{HVP} , is also a particularly interesting example. It requires the determination of the Laplace-like transform:

$$G(x_0) = \int_{\sqrt{t_0}}^{\infty} d\omega \, e^{-\omega x_0} \, \omega^2 \frac{1}{\pi} \text{Im}\Pi^{\text{HVP}}(\omega^2) \quad \text{where} \quad \omega \equiv \sqrt{t}, \quad (6.1)$$

in the full $0 \leq x_0 \leq \infty$ range. LQCD evaluations of $G(x_0)$ with good precision are, however, limited to a restricted x_0 -window because of technical lattice constraints. The *reconstruction approximants* can then be applied to obtain the necessary extrapolation of the $G(x_0)$ function to its full x_0 region, much the same way as we have done for the MUonE proposal. We plan to discuss this in a forthcoming publication.

Acknowledgments

We wish to thank Jérôme Charles for joint work on possible HVP approximants and their application to LQCD evaluations of a_μ^{HVP} , which lead to this work. Discussions with Marc Knecht and Laurent Lellouch on $g_\mu - 2$ in general, have also been very helpful. We are particularly grateful to Jérôme Charles, Marc Knecht and Santi Peris for comments and a careful reading of the manuscript.

A QED Vacuum Polarization as a Theoretical Laboratory

At the one loop level, the QED spectral function of a fermion of arbitrary mass M is given by ¹⁵

$$\frac{1}{\pi} \text{Im}\Pi_{\text{QED}}(t) = \frac{1}{3} \left(1 + \frac{1}{2} \frac{\text{th}}{t} \right) \sqrt{1 - \frac{\text{th}}{t}} \, \vartheta(t - \text{th}), \quad \text{th} \equiv 4M^2, \quad (\text{A.1})$$

¹⁵Notice that this spectral function is the same as the one of the constituent quark model for a quark of mass M . All the relevant equations in this section are in $\frac{\alpha}{\pi}$ units.

and the corresponding photon self-energy function is

$$\Pi_{\text{QED}}(-Q^2) = -\frac{1}{9z^2} \left[(3 - 5z) - 3\sqrt{z(1+z)}(1 - 2z) \arcsin \sqrt{z} \right], \quad z \equiv \frac{Q^2}{\text{th}}. \quad (\text{A.2})$$

The Mellin transform in this case is a ratio of Γ -functions

$$\mathcal{M}_{\text{QED}}(s) = \int_{\text{th}}^{\infty} \frac{dt}{t} \left(\frac{t}{\text{th}} \right)^{s-1} \frac{1}{\pi} \text{Im} \Pi_{\text{QED}}(t) = \frac{\sqrt{\pi}}{4} \frac{\Gamma(3-s)}{(1-s)\Gamma(\frac{7}{2}-s)}, \quad (\text{A.3})$$

with simple poles at $s = 1, 3, 4, \dots$. The coefficients of the Taylor expansion in the ω -disc

$$\Pi_{\text{QED}} \left(-\frac{4\omega}{(1-\omega)^2} \right) \underset{|\omega|<1}{\sim} \sum_{n=1}^{\infty} \Omega_{\text{QED}}(n) \omega^n, \quad (\text{A.4})$$

can then be evaluated analytically using Eq. (2.11):

$$\begin{aligned} \Omega_{\text{QED}}(n) &= \frac{\sqrt{\pi}}{4} \sum_{p=1}^n (-1)^p \frac{4^p \Gamma(n+p)}{\Gamma(2p)\Gamma(n+1-p)} \frac{\Gamma(2+p)}{p \Gamma(\frac{5}{2}+p)} \\ &= \left(-\frac{2}{3} \right) \frac{16n^3 - 40n}{16n^4 - 40n^2 + 9}. \end{aligned} \quad (\text{A.5})$$

In this example we have, therefore, all the ingredients to apply the transfer theorem analytically.

A.1 Reconstruction Approximants in the QED Example

Using the partial fraction expansion

$$\frac{16n^3 - 40n}{16n^4 - 40n^2 + 9} = \frac{9}{8} \frac{1}{2n-1} + \frac{9}{8} \frac{1}{2n+1} - \frac{1}{8} \frac{1}{2n+3} - \frac{1}{8} \frac{1}{2n-3}, \quad (\text{A.6})$$

one can show that for a fixed n , the coefficients $\Omega_{\text{QED}}(n)$ can be written as an infinite series of inverse n -powers ¹⁶:

$$\Omega_{\text{QED}}(n) = \left(-\frac{2}{3} \right) \frac{1}{8} \sum_{p=0}^{\infty} \frac{(9-9^p)}{2^{2p}} \frac{1}{n^{2p+1}}. \quad (\text{A.7})$$

¹⁶This follows from the fact that:

$$\begin{aligned} &\frac{1}{2n-1} + \frac{9}{8} \frac{1}{2n+1} - \frac{1}{8} \frac{1}{2n+3} - \frac{1}{8} \frac{1}{2n-3} \\ &= \frac{1}{8} \left[9 \frac{1}{2n} \sum_{l=0}^{\infty} \left(-\frac{1}{2n} \right)^l + 9 \frac{1}{2n} \sum_{l=0}^{\infty} \left(\frac{1}{2n} \right)^l - \frac{1}{2n} \sum_{l=0}^{\infty} \left(\frac{3}{2n} \right)^l - \frac{1}{2n} \sum_{l=0}^{\infty} \left(-\frac{3}{2n} \right)^l \right] \\ &= \frac{1}{8} \frac{1}{2n} \left[9 \sum_{l=0}^{\infty} \frac{(-1)^l + 1}{2^l n^l} - \sum_{l=0}^{\infty} \frac{3^l + (-3)^l}{2^l n^l} \right] \underset{\text{odd terms}}{=} \underset{\text{sum} \rightarrow 0}{=} \frac{1}{8} \frac{1}{n} \sum_{p=0}^{\infty} \frac{9-3^{2p}}{2^{2p} n^{2p}} = \frac{1}{8} \sum_{p=0}^{\infty} \frac{(9-9^p)}{2^{2p} n^{2p+1}}. \end{aligned}$$

As a result, the asymptotic $\Omega_{\text{QED}}^{\text{AS}}(n)$ series generated by the full non-analytic structure of the $\Pi_{\text{QED}}(-Q^2)$ function in the conformal disc is known:

$$\Omega_{\text{QED}}^{\text{AS}}(n) = -\frac{2}{3} \frac{1}{n} + \frac{3}{8} \frac{1}{n^5} + \frac{15}{16} \frac{1}{n^7} + \frac{273}{128} \frac{1}{n^9} + \mathcal{O}(n^{-11}). \quad (\text{A.8})$$

Retaining only the leading $\mathcal{O}(\frac{1}{n})$ term of this series corresponds to what was done in section III.1. We can now improve on that by including successive terms from the series in Eq. (4.1) up to an arbitrary number of L terms:

$$\Omega_{\text{QED}}^{\text{AS}}(n, L) = \sum_{l=1}^L \frac{\mathcal{B}_l^{\text{QED}}}{n^l}, \quad (\text{A.9})$$

where (for p integer)

$$\mathcal{B}_{2p}^{\text{QED}} = 0 \quad \text{and} \quad \mathcal{B}_{2p-1}^{\text{QED}} = \left(-\frac{2}{3}\right) \frac{1}{8} \frac{9 - 9^{p-1}}{2^{2p-2}}. \quad (\text{A.10})$$

Applying now the definition of the polylogarithm function in Eq. (3.8) to the infinite n -sum

$$\sum_{n=1}^{\infty} \Omega_{\text{QED}}^{\text{AS}}(n, L) \omega^n, \quad (\text{A.11})$$

one gets the corresponding $\Omega_{\text{QED}}^{\text{AS}(L)}(\omega)$ -function as a linear combination of polylog functions, in this case with analytically known coefficients,

$$\sum_{n=1}^{\infty} \Omega_{\text{QED}}^{\text{AS}}(n, L) \omega^n = \Omega_{\text{QED}}^{\text{AS}(L)}(\omega) = \left(-\frac{2}{3}\right) \frac{1}{8} \sum_{p=1}^{\lfloor \frac{L+1}{2} \rfloor} \frac{9 - 9^{p-1}}{2^{2p-2}} \text{Li}_{2p-1}(\omega). \quad (\text{A.12})$$

We conclude that, in this QED example, the *reconstruction approximants* to the lowest order self-energy function which follow from the transfer theorem are:

$$\begin{aligned} \Pi_{\text{QED}}^{\text{N,L}} \left(-\frac{x^2}{1-x} m_\mu^2 \right) &= \sum_{n=1}^N \mathcal{A}_{\text{QED}}(n, L) \left(\frac{\sqrt{1 + \frac{x^2}{1-x} \frac{m_\mu^2}{\text{th}} - 1}}{\sqrt{1 + \frac{x^2}{1-x} \frac{m_\mu^2}{\text{th}} + 1}} \right)^n \\ &+ \sum_{p=1}^{\lfloor \frac{L+1}{2} \rfloor} \mathcal{B}_{2p-1}^{\text{QED}} \text{Li}_{2p-1} \left(\frac{\sqrt{1 + \frac{x^2}{1-x} \frac{m_\mu^2}{\text{th}} - 1}}{\sqrt{1 + \frac{x^2}{1-x} \frac{m_\mu^2}{\text{th}} + 1}} \right), \end{aligned} \quad (\text{A.13})$$

where the coefficients

$$\mathcal{A}_{\text{QED}}(n, L) \equiv \Omega_{\text{QED}}(n) - \Omega_{\text{QED}}^{\text{AS}}(n, L) \quad \text{and} \quad \mathcal{B}_{2p-1}^{\text{QED}}, \quad (\text{A.14})$$

are all known analytically: $\Omega_{\text{QED}}(n)$ in Eq. (A.5), $\Omega_{\text{QED}}^{\text{AS}}(n, L)$ in Eq. (A.9), and $\mathcal{B}_{2p-1}^{\text{QED}}$ in Eq. (A.10).

A.2 Reconstruction Approximants of the QED Spectral Function

The contribution to the imaginary part from the first line of Eq. (A.13) is the same as the one in the first line in Eq. (2.22). The contribution from the polylog sums in the second line of Eq. (A.13) can be obtained from the definition of the phase φ in Eq. (2.18) and the polylog definition in Eq. (3.8):

$$\text{Li}_{2p-1}(e^{i\varphi}) = \sum_{n=1}^{\infty} \frac{e^{in\varphi}}{n^{2p+1}} = \sum_{n=1}^{\infty} \frac{\cos n\varphi}{n^{2p+1}} + i \sum_{n=1}^{\infty} \frac{\sin n\varphi}{n^{2p+1}}. \quad (\text{A.15})$$

The sum which generates the imaginary part can be expressed in terms of the Fourier expansions of the Bernoulli polynomials: $B_{2p-1}(\frac{\varphi}{2\pi})$, because of the well known relation

$$\sum_{n=1}^{\infty} \frac{\sin(n\varphi)}{n^{2p-1}} = (-1)^p \frac{1}{2} \frac{(2\pi)^{2p-1}}{(2p-1)!} B_{2p-1}\left(\frac{\varphi}{2\pi}\right), \quad (\text{A.16})$$

and therefore,

$$\text{Im} [\text{Li}_{2p-1}(e^{i\varphi})] = (-1)^p \frac{1}{2} \frac{(2\pi)^{2p-1}}{(2p-1)!} B_{2p-1}\left(\frac{\varphi}{2\pi}\right). \quad (\text{A.17})$$

All the ingredients to obtain the QED spectral function *reconstruction approximants* are now there, with the result:

$$\begin{aligned} \frac{1}{\pi} \text{Im} \Pi_{\text{QED}}^{\text{N,L}}(t) = & \left\{ -\frac{1}{\pi} \frac{2\sqrt{\frac{t}{t_h} - 1}}{\frac{t}{t_h}} \sum_{n=1}^N \mathcal{A}_{\text{QED}}(n, L) U_{n-1}\left(\frac{t - 2t_h}{t}\right) \right. \\ & \left. + \sum_{p=1}^{\lfloor \frac{L+1}{2} \rfloor} \mathcal{B}_{2p-1}^{\text{QED}} (-1)^{p-1} \frac{(2\pi)^{2p-2}}{(2p-1)!} B_{2p-1}\left(\frac{\pi - 2 \arctan\left(\sqrt{\frac{t}{t_h} - 1}\right)}{2\pi}\right) \right\} \theta(t - t_h). \end{aligned} \quad (\text{A.18})$$

Notice that $\mathcal{B}_3^{\text{QED}} = 0$ due to the fact that in QED the coefficient $\mathcal{R}_{2,1}$ in the corresponding singular series expansion to Eq. (2.6) vanishes. In other words, there is no $\frac{m^2}{Q^2} \log \frac{Q^2}{m^2}$ term¹⁷ in the large- Q^2 expansion of the self-energy $\Pi_{\text{QED}}(-Q^2)$.

In particular, the spectral function approximant when $L=1$ reduces to

$$\begin{aligned} \frac{1}{\pi} \text{Im} \Pi_{\text{QED}}^{\text{N,L=1}}(t) = & \left\{ -\frac{1}{\pi} \frac{2\sqrt{\frac{t}{t_h} - 1}}{\tau} \sum_{n=1}^N \left(\Omega_{\text{QED}}(n) + \frac{\alpha}{\pi} \frac{2}{3} \right) U_{n-1}\left(\frac{t - 2t_h}{t}\right) \right. \\ & \left. + \frac{2}{\pi} \frac{1}{3} \arctan\left(\sqrt{\frac{t}{t_h} - 1}\right) \right\} \theta(t - t_h), \end{aligned} \quad (\text{A.19})$$

¹⁷Incidentally, this is also the case in QCD for the contribution from light quarks in the chiral limit because there is no intrinsic operator of dimension two in QCD. However, as shown in refs. [22–24], this is different for the heavy quarks contributions.

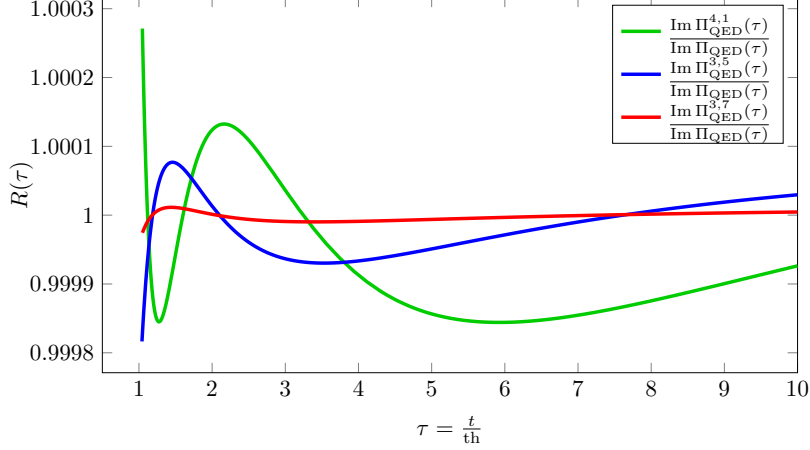


Figure 9. Plot of the ratios of spectral functions in Eq. (A.20). The vertical scale in the figure is very close to the identity.

which is the equivalent QED result to the one discussed in Section III.1.

Numerically, the $\frac{1}{\pi}\text{Im}\Pi_{\text{QED}}^{N,L=1}(t)$ approximants reproduce the exact spectral function in Eq. (A.1) very fast: the shape of the $\frac{1}{\pi}\text{Im}\Pi_{\text{QED}}^{4,1}(\tau)$ approximant for example, already looks identical to the one of $\frac{1}{\pi}\text{Im}\Pi_{\text{QED}}(\tau)$. In order to quantify the quality of the successive *reconstruction approximants*, we plot in Fig (9) the ratios ($\tau = \frac{t}{t_{\text{th}}}$):

$$\frac{\frac{1}{\pi}\text{Im}\Pi_{\text{QED}}^{4,1}(\tau)}{\frac{1}{\pi}\text{Im}\Pi_{\text{QED}}(\tau)}, \quad \frac{\frac{1}{\pi}\text{Im}\Pi_{\text{QED}}^{3,5}(\tau)}{\frac{1}{\pi}\text{Im}\Pi_{\text{QED}}(\tau)}, \quad \frac{\frac{1}{\pi}\text{Im}\Pi_{\text{QED}}^{3,7}(\tau)}{\frac{1}{\pi}\text{Im}\Pi_{\text{QED}}(\tau)} \quad (\text{A.20})$$

respectively in green, blue and red. The figure shows that already the $\frac{1}{\pi}\text{Im}\Pi_{\text{QED}}^{3,7}(\tau)$ approximant is practically a calculation of the QED spectral function in its full τ -range. It also shows that the lower green and blue spectral approximants are not quite locally dual to the physical spectral function; their ratios approach the identity with oscillations which, however, practically disappear in the case of the red approximant. This is an illustration of what was mentioned before about local duality.

B Results on Combinatorial Analysis

B.1 Transfer Theorem

Let us consider a function $f(\omega)$, defined in the the unit disc $|\omega| \leq 1$, which has the asymptotic behaviour

$$f(\omega) \underset{\omega \rightarrow 1}{\sim} (1 - \omega)^m \ln^k \left(\frac{1}{1 - \omega} \right), \quad (\text{B.1})$$

with m and k positive integers. We want to know how this behaviour *transfers* to the coefficients f_n of its Taylor expansion:

$$f(\omega) \underset{|\omega| < 1}{=} \sum_{n=1}^{\infty} f_n \omega^n. \quad (\text{B.2})$$

First we observe that the r.h.s. in Eq. (B.1) can also be written in the following way ($k \geq 1$):

$$(1 - \omega)^m \ln^k \left(\frac{1}{1 - \omega} \right) = \frac{\partial^k}{\partial \varepsilon^k} (1 - \omega)^{m - \varepsilon} \Big|_{\varepsilon=0}. \quad (\text{B.3})$$

Applying to this the inverse Mellin transform representation (the notation $< 0, \infty >$ denotes the fundamental strip where the integral is analytic)

$$(1 - \omega)^a \vartheta(1 - \omega) = \frac{1}{2\pi i} \int_{<0, \infty>} ds \, \omega^{-s} \frac{\Gamma(a+1)\Gamma(s)}{\Gamma(a+1+s)}, \quad \text{with } a = m - \varepsilon \quad \text{and } a > 0, \quad (\text{B.4})$$

one finds that the asymptotic behaviour of Eq. (B.1) can also be written in the following way

$$f(\omega) \underset{\omega \rightarrow 1}{\sim} \frac{\partial^k}{\partial \varepsilon^k} \left(\frac{1}{2\pi i} \int_{<0, \infty>} ds \, \omega^{-s} \frac{\Gamma(m - \varepsilon + 1)\Gamma(s)}{\Gamma(m - \varepsilon + 1 + s)} \right) \Big|_{\varepsilon=0}, \quad (\text{B.5})$$

and therefore [25]

$$f(\omega) \underset{\omega \rightarrow 1}{\sim} \frac{\partial^k}{\partial \varepsilon^k} \left(\sum_{n=0}^{\infty} \frac{(-1)^n}{(m - \varepsilon + 1)_{-n}} \frac{\omega^n}{(1)_n} \right) \Big|_{\varepsilon=0}, \quad (\text{B.6})$$

where we have introduced the Pochhammer symbol [36] notation: $(a)_n \equiv \frac{\Gamma(a+n)}{\Gamma(a)}$. Using the property

$$(m - \varepsilon + 1)_{-n} = \frac{(-1)^n}{(\varepsilon - m)_n}, \quad (\text{B.7})$$

we get

$$f(\omega) \underset{\omega \rightarrow 1}{\sim} \sum_{n=0}^{\infty} \left[\frac{\partial^k}{\partial \varepsilon^k} (\varepsilon - m)_n \right] \Big|_{\varepsilon=0} \frac{\omega^n}{(1)_n}, \quad (\text{B.8})$$

and the question now is to find the asymptotic behaviour for large n of the coefficients

$$\frac{1}{(1)_n} \left[\frac{\partial^k}{\partial \varepsilon^k} (\varepsilon - m)_n \right] \Big|_{\varepsilon=0}. \quad (\text{B.9})$$

The answer to that is given in Eq. (52) of ref.[37]¹⁸:

$$\left[\frac{\partial^k}{\partial \varepsilon^k} (\varepsilon - m)_n \right] \Big|_{\varepsilon=0} \underset{n > m}{=} (-1)^{m+k+1} \Gamma(k+1) \sum_{j=1}^k (-1)^j \begin{bmatrix} m+1 \\ k-j+1 \end{bmatrix} \begin{bmatrix} n-m \\ j \end{bmatrix}, \quad (\text{B.10})$$

where $\begin{bmatrix} a \\ b \end{bmatrix}$ are *unsigned Stirling numbers of the first kind* [27]. The asymptotic behaviour of f_n coefficients is, therefore, proportional to a linear combination of the number symbols

$$\frac{1}{(1)_n} \begin{bmatrix} n-m \\ j \end{bmatrix}, \quad \text{for } 1 \leq j \leq k. \quad (\text{B.11})$$

¹⁸In this reference, the derivative corresponds to the notation $\mathcal{P}_n^{(k)}(-m)$.

When j is an integer, the expressions for these symbols are well-known [27]. They are given in terms of harmonic numbers; for example,

$$\begin{bmatrix} n-m \\ 1 \end{bmatrix} = (-1)^m \frac{\Gamma(n-m)}{\Gamma(1)} \quad (\text{B.12})$$

$$\begin{bmatrix} n-m \\ 2 \end{bmatrix} = (-1)^m \frac{\Gamma(n-m)}{\Gamma(2)} H_{n-m-1} \quad (\text{B.13})$$

$$\begin{bmatrix} n-m \\ 3 \end{bmatrix} = (-1)^m \frac{\Gamma(n-m)}{\Gamma(3)} \left[H_{n-m-1}^2 - H_{n-m-1}^{(2)} \right] \quad (\text{B.14})$$

$$\begin{bmatrix} n-m \\ 4 \end{bmatrix} = (-1)^m \frac{\Gamma(n-m)}{\Gamma(4)} \left[H_{n-m-1}^3 - 3 H_{n-m-1} H_{n-m-1}^{(2)} + 2 H_{n-m-1}^{(3)} \right], \quad (\text{B.15})$$

where

$$H_N^{(r)} = \sum_{j=1}^N \frac{1}{j^r}, \quad \text{and} \quad H_N = H_N^{(1)}, \quad (\text{B.16})$$

are the harmonic numbers; and their large N behaviour are well-known [38]:

$$H_N^{(1)} \underset{N \rightarrow \infty}{\sim} \ln N + \sum_{j=0}^{\infty} \frac{h_j(1)}{N^j} \quad (\text{B.17})$$

$$H_N^{(r>1)} \underset{N \rightarrow \infty}{\sim} \sum_{j=0}^{\infty} \frac{h_j(r)}{N^j}, \quad (\text{B.18})$$

with coefficients

$$h_0(1) = \gamma_E, \quad h_1(1) = \frac{1}{2}, \quad h_j(1) = -\frac{B_j}{j} \cos^2\left(\frac{\pi}{2}j\right) \quad (\text{B.19})$$

$$h_0(r) = \zeta(r), \quad h_{j < r-1}(r) = 0, \quad h_{r-1}(r) = \frac{1}{r-1}, \quad h_r(r) = \frac{1}{2}, \quad (\text{B.20})$$

$$h_{j>r}(r) = -B_j \frac{\Gamma(j+r-1)}{\Gamma(j)\Gamma(r)} \cos^2\left(\frac{\pi}{2}j\right), \quad (\text{B.21})$$

where B_j are the Bernoulli's numbers.

We are still left with the overall factor $\frac{\Gamma(n-m)}{(1)_n}$ in front of each linear combination of harmonic numbers, which has an expansion:

$$\frac{\Gamma(n-m)}{(1)_n} = \frac{\Gamma(n-m)}{\Gamma(n+1)} = \frac{1}{(n-m) \cdots (n-1)n} = \frac{1}{n^{m+1}} \sum_{j=0}^{\infty} \left\{ \begin{matrix} m+j \\ m \end{matrix} \right\} \frac{1}{n^j}, \quad (\text{B.22})$$

where $\left\{ \begin{matrix} a \\ b \end{matrix} \right\}$ are (this time) the *Stirling numbers of the second kind* [27]. Putting all the

expansions together, we have the following results as explicit examples of *transfers*:

$$(1 - \omega)^m \ln \left(\frac{1}{1 - \omega} \right) \mapsto f_n \underset{n \rightarrow \infty}{\sim} \frac{(-1)^m \Gamma(m + 1)}{n^{m+1}} \sum_{j=0}^{\infty} \left\{ \begin{matrix} m + j \\ m \end{matrix} \right\} \frac{1}{n^j} \quad (\text{B.23})$$

$$(1 - \omega)^m \ln^2 \left(\frac{1}{1 - \omega} \right) \mapsto f_n \underset{n \rightarrow \infty}{\sim} \frac{(-1)^m \Gamma(m + 1)}{n^{m+1}} \sum_{j=0}^{\infty} \frac{1}{n^j} \left[\left\{ \begin{matrix} m + j \\ m \end{matrix} \right\} (\ln n + H_m) + \sum_{\ell=0}^j \left\{ \begin{matrix} m + \ell \\ m \end{matrix} \right\} h_{j-\ell}(1) \right], \quad (\text{B.24})$$

where the result in the first line corresponds to Eq. (3.5) in the text.

There is also a general formula for any integers m and k which can be obtained recursively as follows:

$$(1 - \omega)^m \ln^k \left(\frac{1}{1 - \omega} \right) \mapsto f_n \underset{n \rightarrow \infty}{\sim} \frac{(-1)^{m+k+1} \Gamma(k + 1)}{n^{m+1}} \sum_{j=0}^{\infty} \sum_{p=0}^{k-1} g_{j,p}(m, k) \frac{\ln^p n}{n^j}, \quad (\text{B.25})$$

where

$$g_{j,p}(m, k) = \sum_{b=0}^j \sum_{a=1}^{p+1} \frac{(-1)^a}{\Gamma(a)} \left\{ \begin{matrix} m + j - b \\ m \end{matrix} \right\} \left[\begin{matrix} m + 1 \\ k - a + 1 \end{matrix} \right] w_j(b - 1, p), \quad (\text{B.26})$$

and the coefficients $w_j(M, p)$ defined by recursive relations

$$w_j(M + 1, M + 1) = w_j(M, M) \quad (\text{B.27})$$

$$w_j(M + 1, 0) = \sum_{b=0}^j \sum_{c=0}^M (-M)_c h_{j-b}(c + 1) w_j(M - c, 0) \quad (\text{B.28})$$

$$w_j(M + 1, p \geq 1) = w_j(M, p - 1) + \sum_{b=0}^j \sum_{c=0}^{M-p} (-M)_c h_{j-b}(c + 1) w_j(M - c, p). \quad (\text{B.29})$$

We find, in particular, that the leading term in the r.h.s. of Eq. (B.25) is given by the simple expression:

$$f_n \underset{n \rightarrow \infty}{\sim} (-1)^m \Gamma(m + 1) k \frac{\ln^{k-1} n}{n^{m+1}} + \mathcal{O} \left(\frac{\log^{k-2} n}{n^{m+1}} \right). \quad (\text{B.30})$$

B.2 Relation between the \mathcal{B} -coefficients and the \mathcal{R} -residues

Let us start with the asymptotic expansion

$$\Pi \left(-\frac{4\omega}{(1 - \omega)^2} \right) \underset{\omega \rightarrow 1}{\sim} \sum_{m \geq 0} \tilde{\mathcal{R}}_{m,1} (1 - \omega)^m \ln \left(\frac{1}{1 - \omega} \right). \quad (\text{B.31})$$

The application of the transfer theorem to the r.h.s. gives the result for the large n behaviour of the Taylor coefficients:

$$(1 - \omega)^m \ln \left(\frac{1}{1 - \omega} \right) \mapsto f_n \underset{n \rightarrow \infty}{\sim} \frac{(-1)^m \Gamma(m + 1)}{n^{m+1}} \sum_{j=0}^{\infty} \left\{ \begin{matrix} m + j \\ m \end{matrix} \right\} \frac{1}{n^j}, \quad (\text{B.32})$$

and therefore

$$\Omega_n^{\text{AS}} = \sum_{j=0}^{\infty} \sum_{m \geq 0} \tilde{\mathcal{R}}_{m,1} \left\{ \begin{matrix} m+j \\ m \end{matrix} \right\} \frac{(-1)^m \Gamma(m+1)}{n^{m+1+j}}. \quad (\text{B.33})$$

Recall next the definition of the \mathcal{B}_l -coefficients in the text:

$$\Omega_n^{\text{AS}} = \sum_{l=0}^{\infty} \frac{\mathcal{B}_l}{n^l}. \quad (\text{B.34})$$

Separating the first term in Eq. (B.33), we have

$$\Omega_n^{\text{AS}} = \frac{-2\mathcal{R}_{1,1}}{n} + \sum_{j=0}^{\infty} \sum_{m \geq 1} \tilde{\mathcal{R}}_{m,1} \left\{ \begin{matrix} m+j \\ m \end{matrix} \right\} \frac{(-1)^m \Gamma(m+1)}{n^{m+1+j}}, \quad (\text{B.35})$$

and therefore

$$\mathcal{B}_1 = -2\mathcal{R}_{1,1}. \quad (\text{B.36})$$

Performing the change of variable: $l = m + 1 + j$ in the second term of Eq. (B.35) results in the expression

$$\begin{aligned} & \sum_{j=0}^{\infty} \sum_{m \geq 1} \tilde{\mathcal{R}}_{m,1} \left\{ \begin{matrix} m+j \\ m \end{matrix} \right\} \frac{(-1)^m \Gamma(m+1)}{n^{m+1+j}} \\ &= \sum_{l=2}^{\infty} \sum_{j=0}^{\infty} \sum_{m \geq 1} \tilde{\mathcal{R}}_{m,1} \left\{ \begin{matrix} m+j \\ m \end{matrix} \right\} \frac{(-1)^m \Gamma(m+1)}{n^{m+1+j}} \delta(m+1+j-l) \vartheta(j), \end{aligned} \quad (\text{B.37})$$

and reorganizing the sums with the use of the δ -function argument, we get

$$\sum_{j=0}^{\infty} \sum_{m \geq 1} \tilde{\mathcal{R}}_{m,1} \left\{ \begin{matrix} m+j \\ m \end{matrix} \right\} \frac{(-1)^m \Gamma(m+1)}{n^{m+1+j}} = \sum_{l=2}^{\infty} \sum_{m=1}^{l-1} \tilde{\mathcal{R}}_{m,1} \left\{ \begin{matrix} l-1 \\ m \end{matrix} \right\} \frac{(-1)^m \Gamma(m+1)}{n^l} \quad (\text{B.38})$$

and therefore, by identification with Eq. (B.34), the wanted results:

$$\mathcal{B}_1 = -2\mathcal{R}_{1,1} \quad (\text{B.39})$$

$$\mathcal{B}_l = \sum_{m=1}^{l-1} \tilde{\mathcal{R}}_{m,1} \left\{ \begin{matrix} l-1 \\ m \end{matrix} \right\} (-1)^m \Gamma(m+1). \quad (\text{B.40})$$

Using the relation

$$\tilde{\mathcal{R}}_{m,1} = -2 \sum_{\mathfrak{p}=2}^{\lfloor \frac{m+2}{2} \rfloor} \binom{m-\mathfrak{p}}{\mathfrak{p}-2} 4^{1-\mathfrak{p}} \mathcal{R}_{\mathfrak{p},1}, \quad (\text{B.41})$$

we have

$$\mathcal{B}_l = -2 \sum_{m=1}^{l-1} \sum_{\mathfrak{p}=2}^{\lfloor \frac{m+2}{2} \rfloor} \left\{ \begin{matrix} l-1 \\ m \end{matrix} \right\} (-1)^m \Gamma(m+1) \binom{m-\mathfrak{p}}{\mathfrak{p}-2} 4^{1-\mathfrak{p}} \mathcal{R}_{\mathfrak{p},1}, \quad (\text{B.42})$$

and more explicitly, up to $l = 5$:

$$\mathcal{B}_2 = 0 \quad (\text{B.43})$$

$$\mathcal{B}_3 = \mathcal{R}_{2,1} \quad (\text{B.44})$$

$$\mathcal{B}_4 = 0 \quad (\text{B.45})$$

$$\mathcal{B}_5 = \mathcal{R}_{2,1} + 3\mathcal{R}_{3,1} , \quad (\text{B.46})$$

which are the terms that we have been using in the numerical applications.

The fact that all the l -even coefficients \mathcal{B}_l vanish, follows from Eq. (B.42), but there is an interesting reason for that. This property is related to the fact that the vacuum polarization self-energy, as a function of the conformal ω -variable, is invariant under the transformation $\omega \mapsto \frac{1}{\omega}$:

$$\Pi\left(-\frac{4\omega}{(1-\omega)^2}\right) \mapsto \Pi\left(-\frac{4\frac{1}{\omega}}{(1-\frac{1}{\omega})^2}\right) = \Pi\left(-\frac{4\omega}{(1-\omega)^2}\right) . \quad (\text{B.47})$$

Formally, for its Taylor series in Eq. (2.10), this implies

$$\sum_{n=1}^{\infty} \Omega_n \omega^n = \sum_{n=1}^{\infty} \Omega_n \left(\frac{1}{\omega}\right)^n = \sum_{n=1}^{\infty} \Omega_{-n} \omega^n , \quad (\text{B.48})$$

and using the relation in Eq. (2.11) between the Ω_n -coefficients and the Mellin moments:

$$\Omega_n = \sum_{p=1}^{\infty} (-1)^p \mathcal{M}(1-p) \frac{4^p \Gamma(n+p)}{\Gamma(2p) \Gamma(n+1-p)} = \sum_{p=1}^{\infty} (-1)^p \mathcal{M}(1-p) 4^p \binom{n+p-1}{2p-1} , \quad (\text{B.49})$$

it is easy to show from properties of the binomial coefficient, that

$$\Omega_n = -\Omega_{-n} ; \quad (\text{B.50})$$

i.e. Ω_n is an odd function of n . Therefore, in the case were the Mellin transform has only single poles, which has been assumed in this paper, there follows that

$$\Omega_n \underset{n \rightarrow \infty}{\sim} \Omega_n^{\text{AS}} = \sum_{l=1}^{\infty} \frac{\mathcal{B}_l}{n^l} = -\Omega_{-n}^{\text{AS}} = -\sum_{l=1}^{\infty} \frac{(-1)^l \mathcal{B}_l}{n^l} , \quad (\text{B.51})$$

which for k integer, implies $\mathcal{B}_{2k} = 0$.

References

- [1] G. Bennett *et al.*, *Final report of the muon E281 anomalous magnetic moment measurement at BNL*, Phys. Rev. **D73** 072003 (2006).
- [2] B. Abi *et al.* (Muon g-2 Collaboration), Phys.Rev. Lett. **126** 141801 (2021).
- [3] T. Albahri *et al.*, Phys. Rev. **D103**, 072002 (2021).

- [4] T. Aoyama *et al* (Muon g-2 Theory Initiative), *The anomalous magnetic moment of the muon in the Standard Model*, Phys. Rep. **887** 1 (2020).
- [5] Interesting as they may be, there is no space to quote them all here.
- [6] Sz. Borsanyi, Z. Fodor, J.N. Guenther, C. Hoelbling, S.D. Katz, L. Lellouch, T. Lippert, K. Miura, K.K. Szabo, L. Parato, F. Stokes, B.C. Toth, Cs. Torok, L. Varnhorst, *et al* (BMW Collaboration), *Leading hadronic contribution to the muon magnetic moment from lattice QCD*, Nature **593** 51 (2021).
- [7] M. Davier, A. Hoecker, B. Malaescu and Z. Zhang, Eur.Phys.J **C 80** 241 (2020), [Erratum: Eur.Phys.J. **C 80** 410 (2020)].
- [8] A. Keshavarzi, D. Nomura and T. Teubner, Phys. Rev. **D101** 014029 (2020).
- [9] M. Abe *et al*, *A new approach for measuring the muon anomalous magnetic moment and electric dipole moment*, Prog. Theor. Exp. Phys. **2019**, O53C02 (2019).
- [10] C. M. Carloni Calame, M. Passera, L. Trentadue and G. Venanzoni, Phys. Lett. **B746** 325 (2015).
- [11] G. Abbiendi *et al*, Eur. Phys. J, **C77** (2017) 139 (2017).
- [12] G. Abbiendi *et al* Letter of Intent: The MUonE Project, CERN-SPSC-2019-026 / SPSC-I-252 (2019).
- [13] P. Banerjee *et al*, Eur.Phys.J. **80** 6 (2020).
- [14] C. Bouchiat and L. Michel, J. Phys. Radium **22** 121 (1961).
- [15] S.J. Brodsky and E. de Rafael, Phys. Rev. **168** 1620 (1968).
- [16] M. Gourdin and E. de Rafael, Nucl. Phys. **B10** 667 (1969).
- [17] B.E. Lautrup, A. Peterman and E. de Rafael, Phys. Rep. **C3** 193 (1972).
- [18] E. de Rafael, Phys. Lett. **B322** 239 (1994).
- [19] T. Blum, Phys. Rev. **91** 052001 (2003).
- [20] Ph. Flajolet and A.M. Odlyzko, *Singularity analysis of generating functions*, SIAM Journal Discrete Math. **3 2** 216 (1990).
- [21] Philippe Flajolet and Robert Sedgewick, *Analytic Combinatorics*, Cambridge University Press, 2009.
- [22] D. Greynat and S. Peris, Phys. Rev. **D82** 034030 (2010).
- [23] D. Greynat, P. Masjuan and S. Peris, Phys. Rev. **D85** 054008 (2012).
- [24] D. Greynat and P. Masjuan, *PoS, Confinement X*, 162 (2012).
- [25] Ph. Flajolet, X. Gourdon and Ph. Dumas, Theor. Comput. Sci. **144** 3 (1994).
- [26] J. Charles, E. de Rafael and D. Greynat, Phys. Rev. **D97** 076014 (2018).
- [27] V. Adamchik, *On Stirling numbers and Euler sums*, Journal Of Computational And Applied Mathematics, **79**, 119 (1997).
- [28] M.A. Shifman, A.I. Vainshtein and V.I. Zakharov, Nucl. Phys. **B147** 385, 447 (1979).
- [29] M.A. Benitez-Rathgeb, D. Boito, A.H. Hoang and M. Jamin, ArXiv:2111.09614v1 [hep-ph].
- [30] A. Pich and J. Portoles, Phys. Rev. **D63** 093005 (2001).

- [31] G. Colangelo, M. Hoferichter, B. Kubis, M. Niehus and J. Ruiz de Elvira, arXiv:2110.05493v1 [hep-ph].
- [32] C.M. Carloni Calame, *Monte Carlo for the MUonE experiment*, talk at “Flavour Changing and Conserving Processes” (2019).
- [33] G. Abbiendi, *Status of the MUonE experiment*, arXiv:2201.13177v1 [physics,ins-det] (2022).
- [34] E. Balzani, S. Laporta and M. Passera, arXiv:2112.05704v1 [hep-ph].
- [35] D. Bernecker and H.B. Meyer, Eur. Phys. J. **47A** 148 (2011).
- [36] L. Slater *Generalized Hypergeometric Functions*, Cambridge University Press, 1966.
- [37] D. Greynat, J. Sesma and G. Vulvert, J. Math. Phys. **55**, 043501 (2014).
- [38] Grünberg, D.B. *On Asymptotics, Stirling Numbers, Gamma Function and Polylogs*, Result. Math. **49**, 89-125 (2006).